Electronic Supporting Information (ESI)

Molecular diversity in several pyridyl based Cu(II) complexes: Biophysical interaction and red-ox triggered fluorescence switch

Sangita Adhikari[a], Animesh Sahana[a], Babli Kumari[a],Durba Ganguly[b], Saurabh Das[b], Prajna Paramita Banerjee[c], Gautam Banerjee[c], Ansuman Chatterjee[c], Jesús Sanmartín Matalobos*[d], Paula Brandão,[e] Vítor Félix[e,f*] and Debasis Das[a*]

[a]Department of Chemistry, The University of Burdwan, Burdwan, WestBengal, India

[b]Department of Chemistry, Jadavpur University, Kolkata-700032, India

[c]Department of Zoology, Visva Bharati University, Santiniketan, West Bengal, India.

[d]Departamento de QuimicaInorganica,Facultade de Quimica, Avda. DasCiencias s/n, 15782 Santiago de Compostela, Spain.

[e]Department of Chemistry, CICECO – Aveiro Institute of Materials, 3810-193 Aveiro, Portugal.

[f]Department of Medical Sciences, iBiMED – Institute of Biomedicine, University of Aveiro, 3810-193 Aveiro, Portugal.

Contents

1. General method: UV-Vis and fluorescence titration
2. Determination of binding constant
3. Calculation of the detection limit
4. Studies on interaction of c t DNA with **C1a** using UV-Vis spectroscopy
5. Fig. S1. X-ray structure of **L1**with the thermal ellipsoids drawn at the 30% probability level
6. Fig. S2. Perspective view of $[Cu(py)_2(H_2O)(SO_4)]$**.**$2H_2O$ (**C1a)**with the thermal ellipsoids drawn at the 70% probability level showing the copper(II) octahedral coordination sphere exhibited by the two independent molecules. The hydrogen bonds are drawn as green dashed lines.
7. Fig. S3. Perspective views of the repeating units in polymeric chains $[Cu_2(\mathbf{L^1})_2(H_2O)_3Cl_2]$ (top) and $[Cu_2(\mathbf{L^1})_2(H_2O)_3(NO_3)_2]$ (bottom)of C1B showing the relevant atomic notation scheme. Thermal ellipsoids are drawn at the 50% probability level. * and ** stand for the symmetry operations 3/2-*x*,-*y*,1/2-*z* and +*x*,-1/4-*y*,3/4-*z*, respectively.
8. Fig. S4. Molecular structureof $[Cu_2(L4)_4(H_2O)_2]$**.**$1.12(H_2O)$ (**C4**) with thermal ellipsoids drawn at the 70% of probability level showing the octahedral copper centres assembled by four NN ligands. The disordered naphthyle-2-ylmethyl substituents are shown in the position with slightly higher occupancy of 55%. The hydrogen bonds between the coordinated and crystallization water molecules are drawn as green dashed lines.

9. Fig. S5 TGA and DTA plot of **C1a**
10. Fig. S6 TGA and DTA plot of **C1b**
11. Fig. S7Thermogramof **C2**
12. Fig. S8Thermogram of **C3**
13. Fig. S9 TGA and DTA plot of **C4**
14. Fig. S10 PXRD pattern of **C1a**
15. Fig. S11 PXRD pattern of **C1b**
16. Fig. S12 PXRD pattern of **C4**
17. Fig. S13Benesi-Hildebrand plot for measurement of binding constant of **L1** with Cu^{+}
18. Fig. S14Stern-Volmer plot for determination of quenching constant of **L1** for Cu^{2+}
19. Fig. S15Stern-Volmer plot for determination of quenching constant of **L2** for Cu^{2+}
20. Fig. S16 Stern-Volmer plot for determination of quenching constant of **L3** for Cu^{2+}
21. Fig. S17 Stern-Volmer plot for determination of quenching constant of **L4** for Cu^{2+}
22. Fig. S18Bar diagram showing interference of other cations for determination of Cu^{+} using **L1**
23. Fig. S19Job's plot for determination of stoichiometry of interaction between **L1** and Cu^{+}.
24. Fig. S20 ESI-MS of mixtureof**L1** and Cu^{+} in solution
25. Fig. S21. Emission intensity of **L1** as function of added Cu^{+}
26. Fig. S22 Double-reciprocal plot for the evaluation of the apparent binding constant of **C1a** for c t DNA based on UV-Vis titration
27. Fig. S23 Cyclic voltammogram of Cu^{2+} complexes in acetonitrile
28. Fig. S24 ESI-MS of **L2**
29. Fig. S25 UV-Vis spectrum of **L2** in acetonitrile.
30. Fig. S26 FTIR spectrum of **L2**
31. Fig. S27 ^{1}HNMR spectrum of **L2** in $CDCl_3$
32. Fig. S28^{13}CNMR spectrum of **L2** in $CDCl_3$
33. Fig. S29 ESI-MS of **L4**
34. Fig. S30 UV-Vis spectrum of **L4** in acetonitrile.
35. Fig. S31 FTIR spectrum of **L4**
36. Fig. S32^{1}HNMR spectrum of **L4** in DMSO-d_6
37. Fig. S33^{13}CNMR spectrum of **L4** in DMSO-d_6
38. Fig. S34 FTIR spectrum of **C1a**
39. Fig. S35 UV-Vis spectrum of **C1a** in acetonitrile
40. Fig. S36 FTIR spectrum of **C2**
41. Fig. S37 ESI-MS of **C2**
42. Fig. S38FTIR spectrum of **C3**
43. Fig. S39 ESI-MS of **C3**
44. Fig. S40 UV-Vis spectrum of **C3** in acetonitrile
45. Fig. S41 FTIR spectrum of **C4**
46. Table S1. Bond lengths and bond angles in the Cu(II) coordination sphere of C1a
47. Table S2. Hydrogen bond dimensions of C1a
48. Table S3. Selected bond lengths (Å) and bond angles (º) of C1b
49. Table S4. Selected bond lengths (Å) and bond angles (º) of C4

50. Table S5. Crystal data and selected refinement parameters of L1, C1a, C1b and C4.
51. References

General method of UV-Vis and fluorescence titration

Path length of the cells used for absorption and emission studies is 1 cm. 1 μM stock solution of **C1a** is prepared in acetonitrile/ water (1/1, v/v). Working solutions of ascorbic acid are prepared from their respective stock solutions. Emission studies of **L1** with $Cu(MeCN)_4]ClO_4$ is done in acetonitrile solution. Fluorescence measurements are performed using 1nm x 1 nm slit width. Fluorescence spectra are recorded after 40 min of mixing of **C1** with ascorbic acid solution.

Determination of binding constant

The binding constant of L1 for $[Cu^+]$ is determined using a modified Benesi–Hildebrand equation1: $(I_{max} - I_0)/(I - I_0) = 1 + (1/K)\ (1/[C]^n)$ where I_{max}, I_0 and I are emission intensity values for L1 in the presence of $[Cu^+]$ at saturation, in the absence of $[Cu^+]$ and at any intermediate $[Cu^+]$ concentrations, respectively. A plot of $(I_{max} - I_0)/(I - I_0) = 1 + (1/K)\ (1/[C]^n)$ (here n = 1) yields the binding constant value from the slope.

Calculation of the detection limit

Fluorescence titration of **L1**with Cu^+ is carried out by adding aliquots of μMconcentration of Cu^+ to **L1**. The detection limit is obtained as the concentration, at which a sharp change in the emission intensity occurred, multiplied by the concentration of **L1**:[1] $DL = C_L \times C_T$, where C_L is the concentration of **L1,** C_T is the concentration of Cu^+ at which fluorescence enhanced. Thus: DL = 1 μM × 50 μM = 50 μM

Studies on interaction of c t DNA with C1 using UV-Vis spectroscopy

Interaction of c t DNA with **C1a** was studied with the help of UV-Vis spectroscopy [JASCO V-630 UV-Vis spectrophotometer]. Quartz cuvettes from STARNA Scientific Ltd (10mm×10mm) were used. Separate aliquots, containing a constant concentration of **C1a** (100 μM) and gradually increasing concentrations of c t DNA were used at pH 7.4. The total volume was constant (2.0 mL) using 20 mM Tris buffer and 120 mM NaCl, 35 mM KCl and 5 mM $MgCl_2$. When saturation was reached the concentration of c t DNA was ~ 15 folds greater than the complex. The titration was repeated thrice. Binding constant and site size of interaction was determined using standard equations.[2-15]

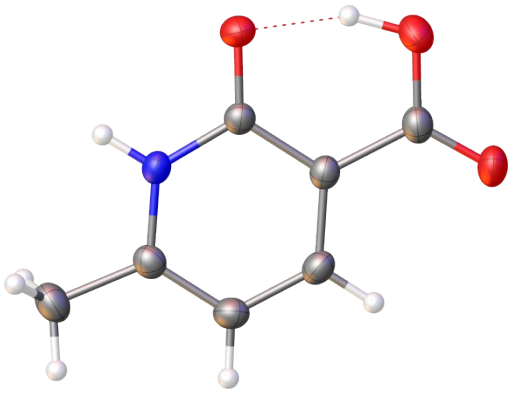

Fig. S1. X-ray structure of **L1**[16] with thermal ellipsoids at 30% probability level

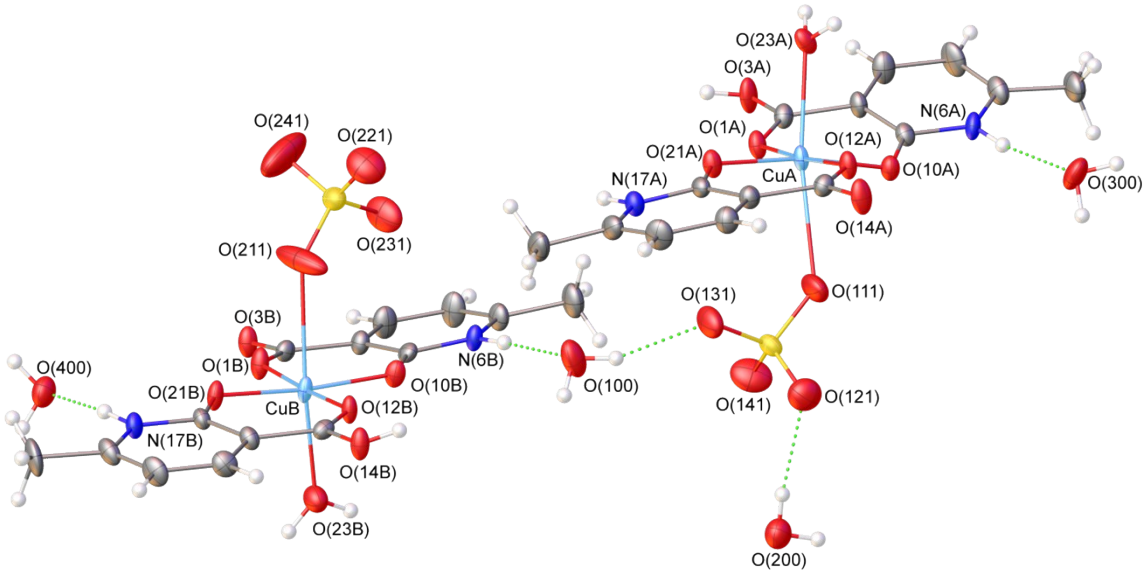

Fig. S2. Perspective view[16] of asymmetric unit of $[Cu(py)_2(H_2O)(SO_4)].2H_2O$ (**C1a)** with thermal ellipsoids at 70% probability level showing Cu(II) octahedral coordination sphere exhibited by two independent molecules. The hydrogen bonds are drawn as green dashed lines.

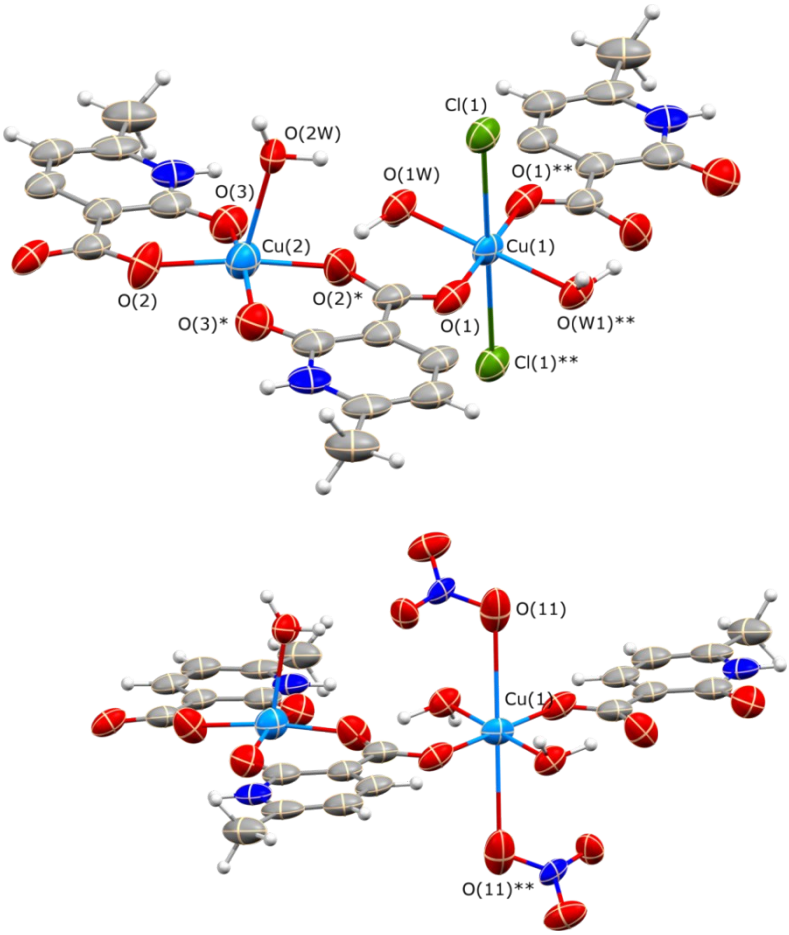

Fig. S3.Perspective views of the repeating units in polymeric chains $[Cu_2(\mathbf{L^1})_2(H_2O)_3Cl_2]$ (top) and $[Cu_2(\mathbf{L^1})_2(H_2O)_3(NO_3)_2]$ (bottom) of **C1B** showing relevant atomic notation scheme. Thermal ellipsoids are drawn at 50% probability level.* and ** stand for the symmetry operations 3/2-*x*,-*y*,1/2-*z* and +*x*,-1/4-*y*,3/4-*z*, respectively

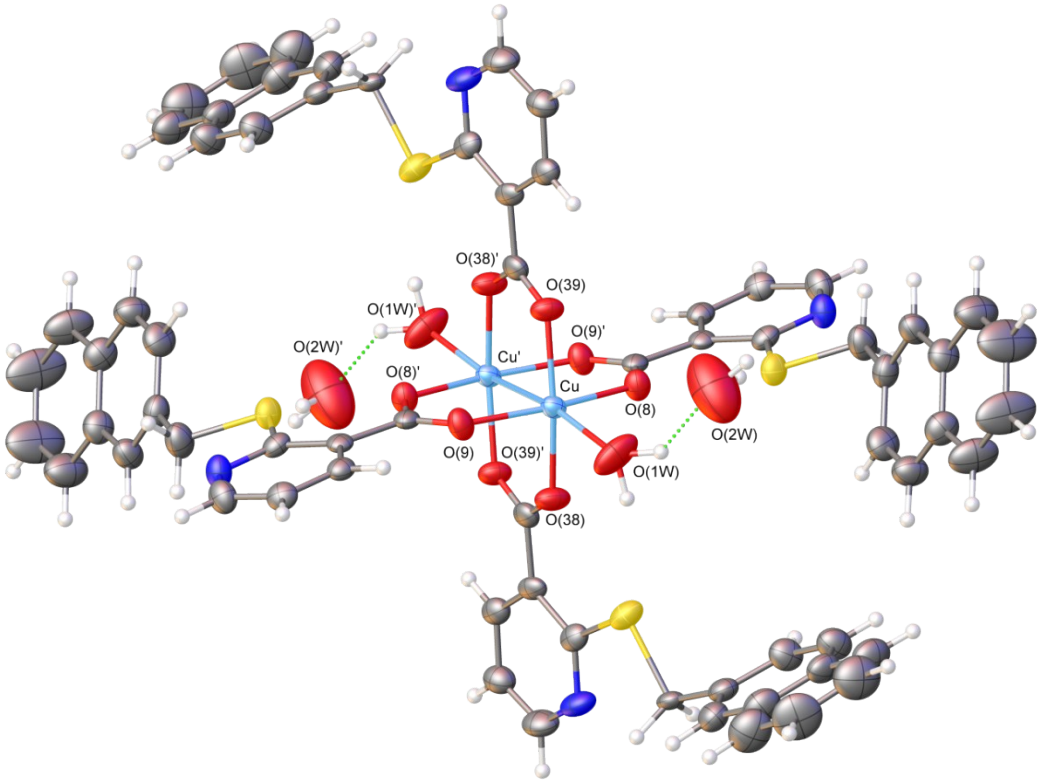

Fig. S4. Molecular structure of $[Cu_2(L4)_4(H_2O)_2]$.1.12(H_2O) (**C4**)[16] with thermal ellipsoids drawn at 70% probability level showing octahedral copper centres assembled by four ligands. The disordered naphthyle-2-ylmethyl substituents are shown in the position with slightly higher occupancy of 55%. The hydrogen bonds between coordinated and crystallization water molecules are drawn as green dashed lines.

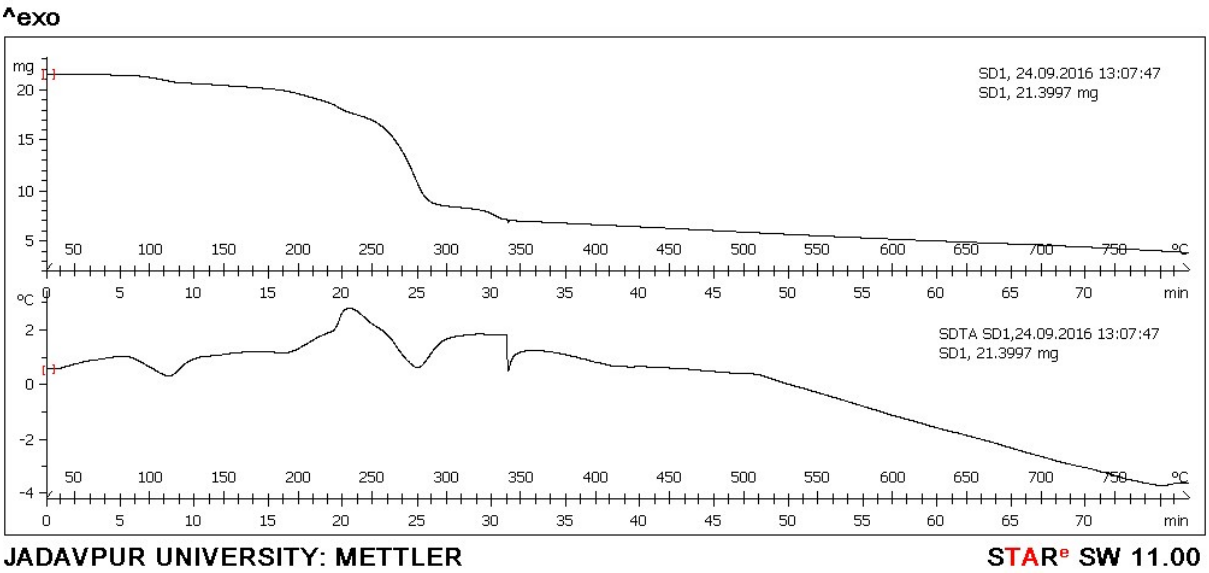

Fig. S5. TGA and DTA plot of **C1a**

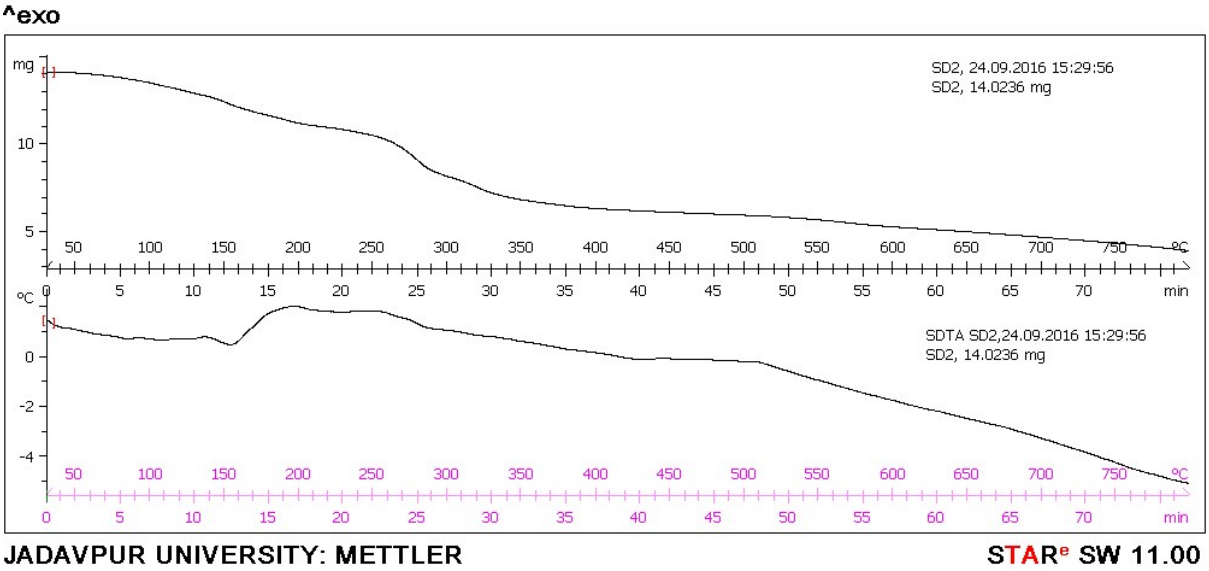

Fig. S6. TGA and DTA plot of **C1b**

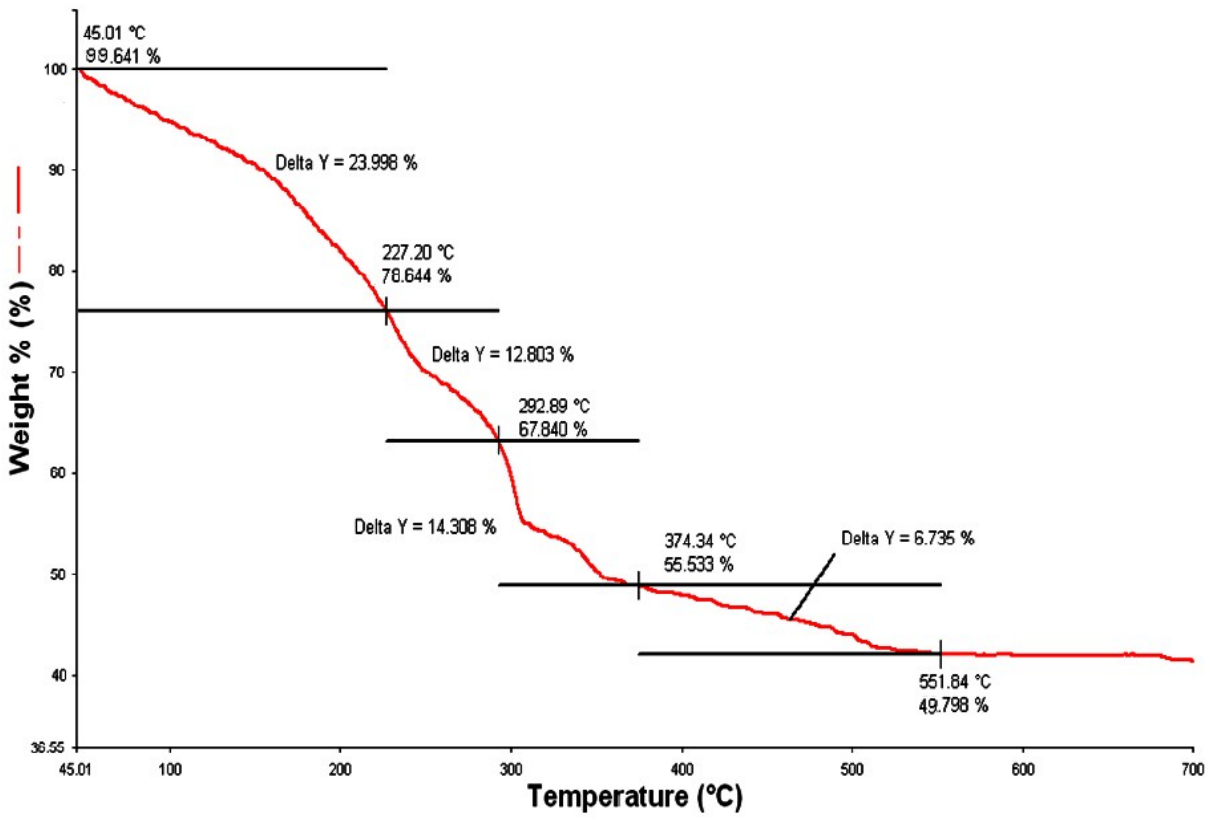

Fig. S7. Thermogram of **C2**

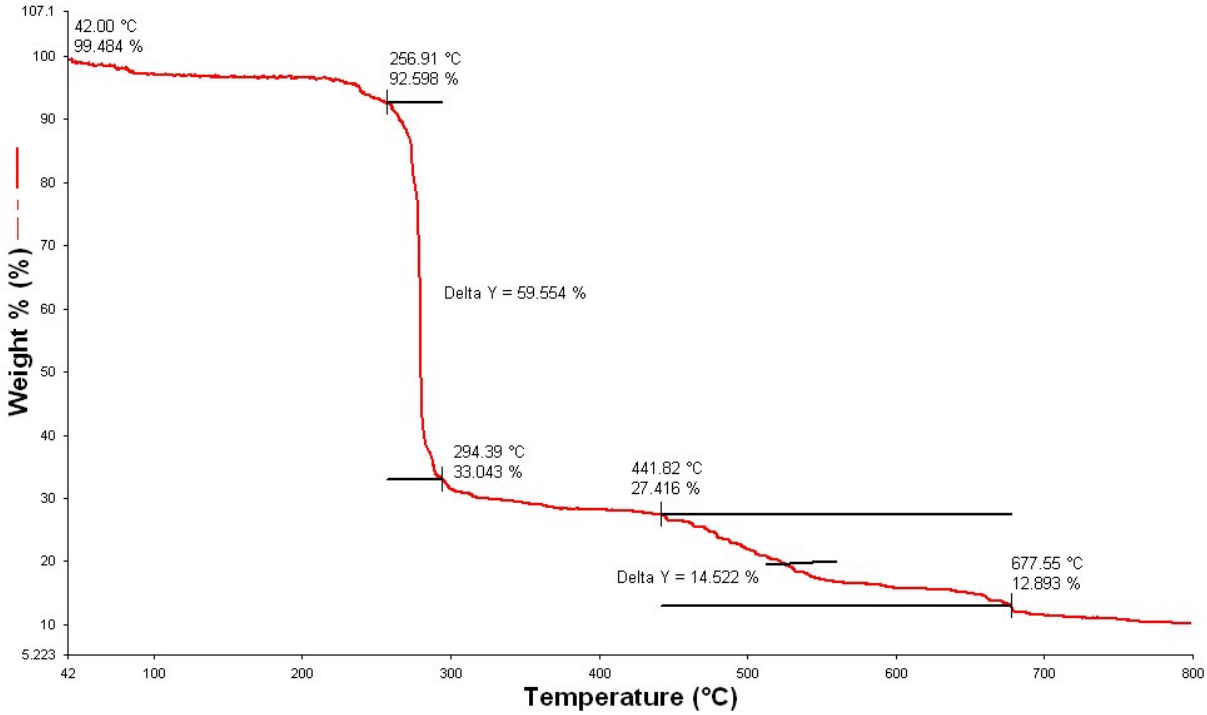

Fig. S8. Thermogram of **C3**

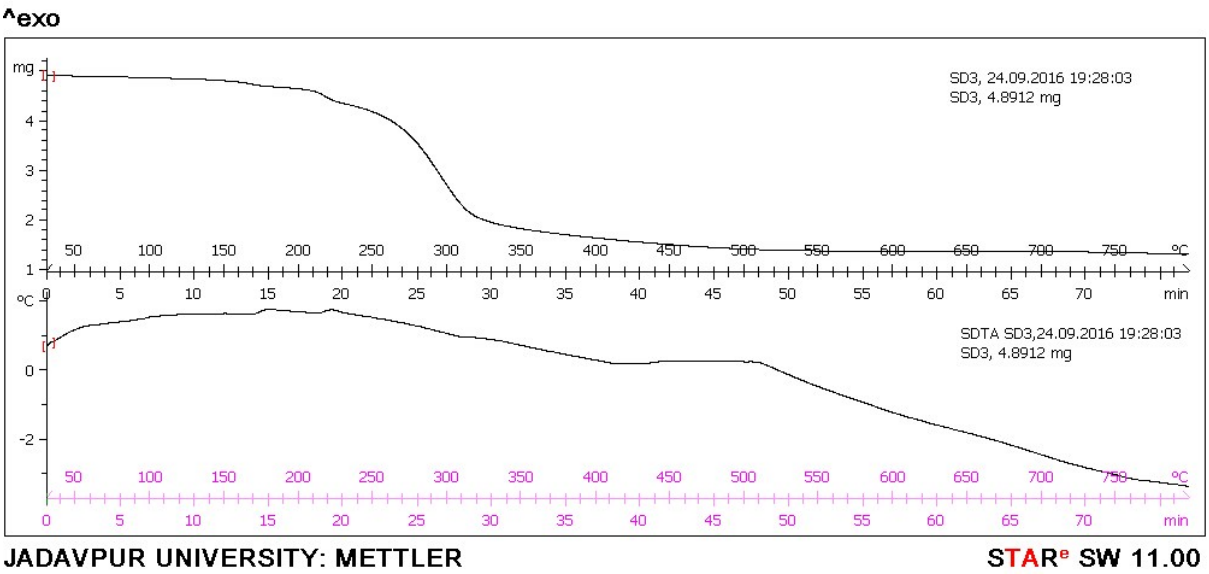

Fig. S9. TGA and DTA plot of **C4**

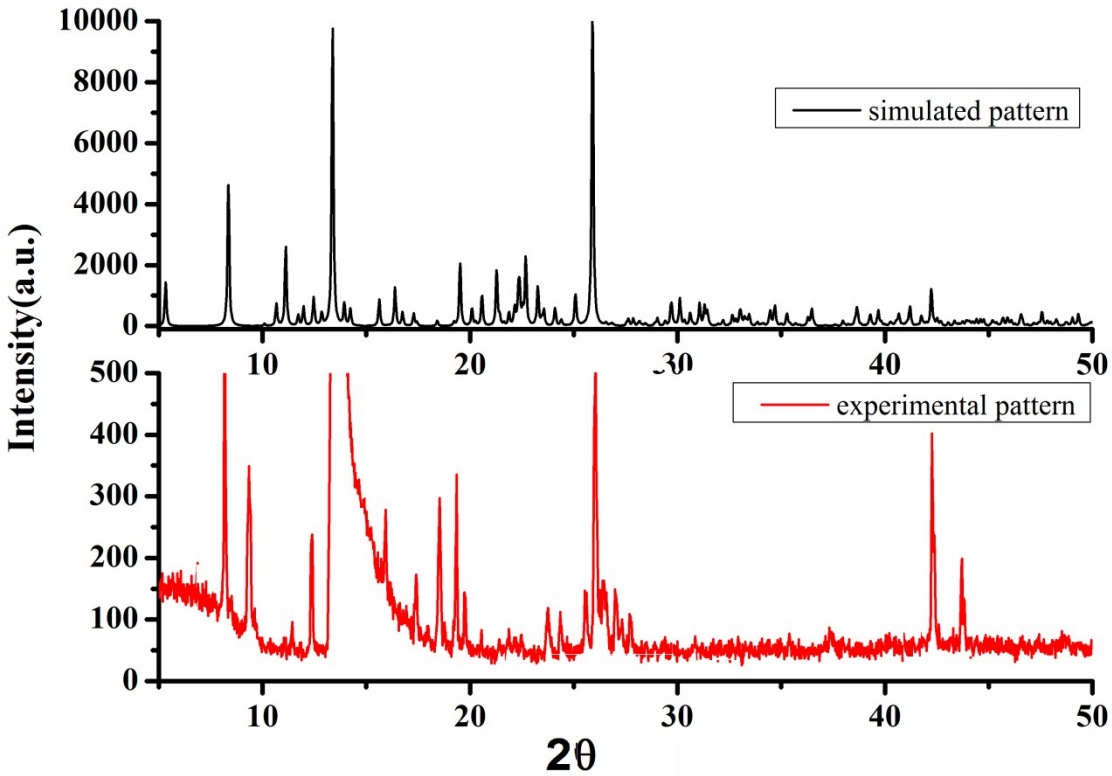

Fig. S10 PXRD pattern of **C1a**

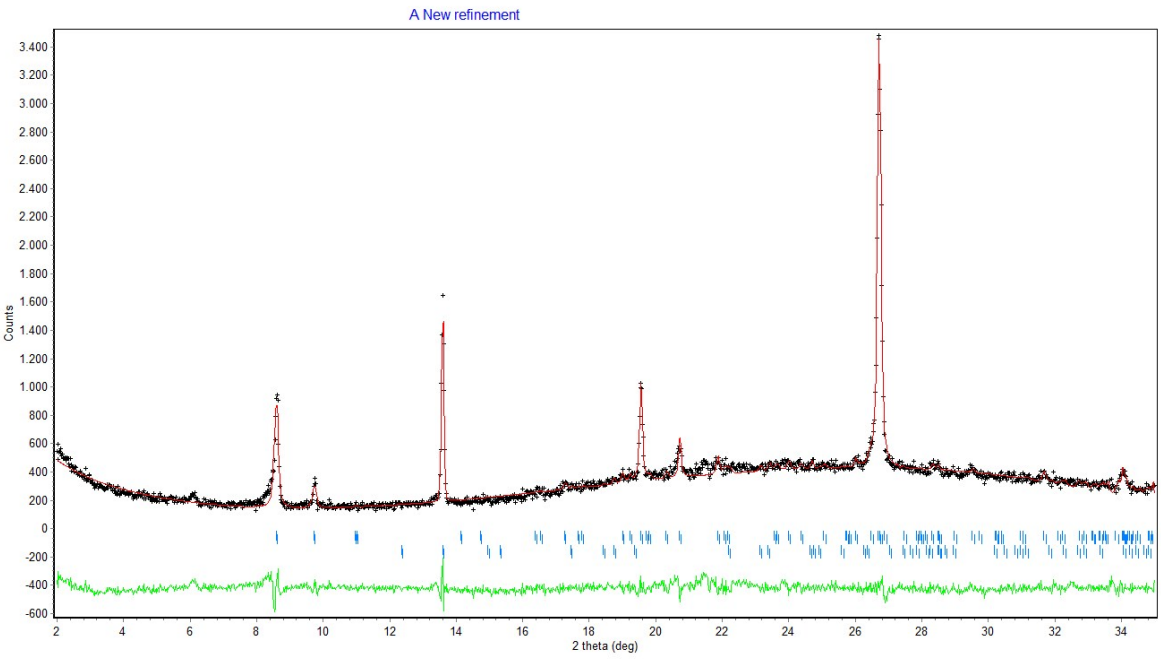

Fig. S11 PXRD pattern of **C1b** experimental diffractogram: black points; simulated diffractogram: red line.

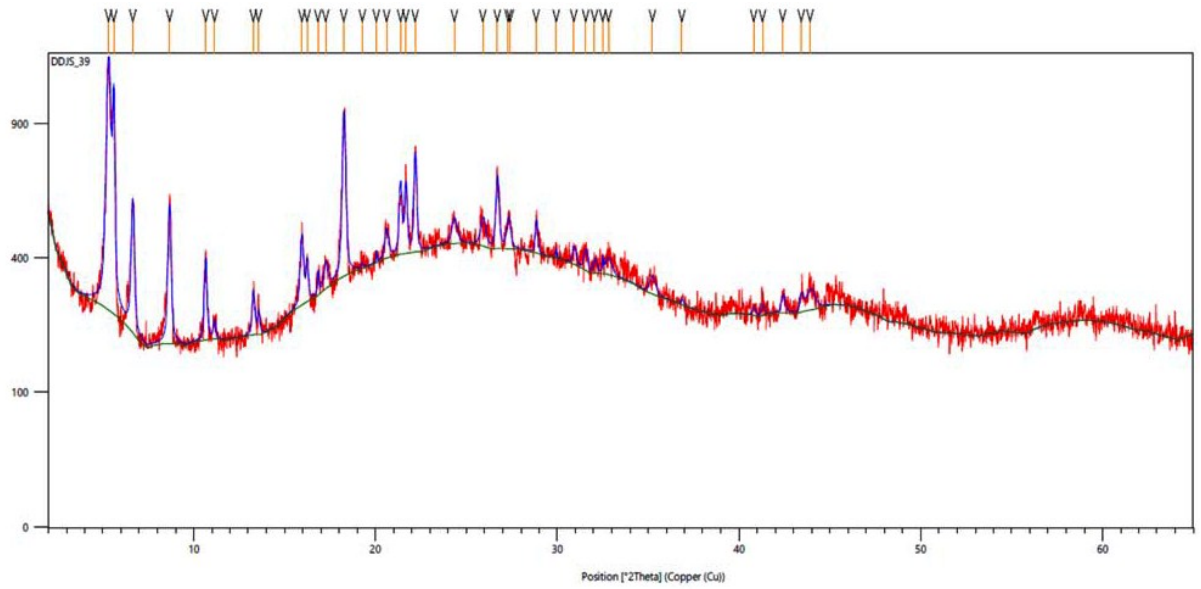

Fig. S12 PXRD pattern of C4; experimental diffractogram: red points; simulated difractogram: blue line.

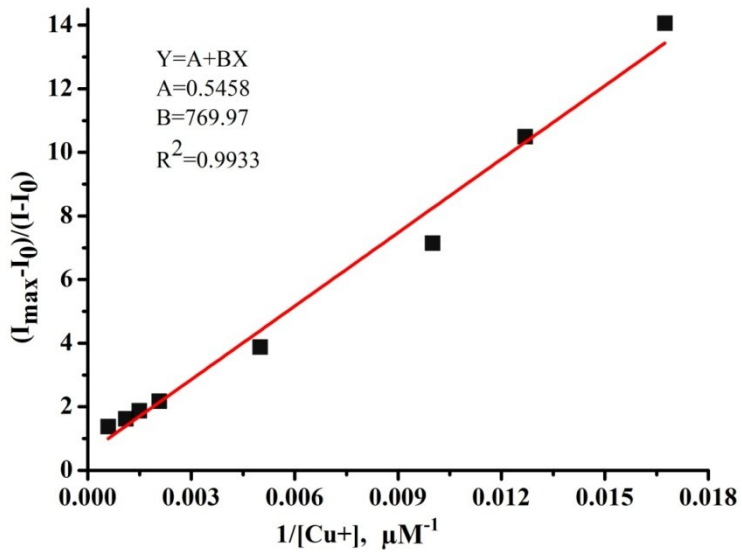

Fig.S13. Benesi-Hildebrand plot for determination of association constant of **L1** with $Cu(MeCN)_4]ClO_4$

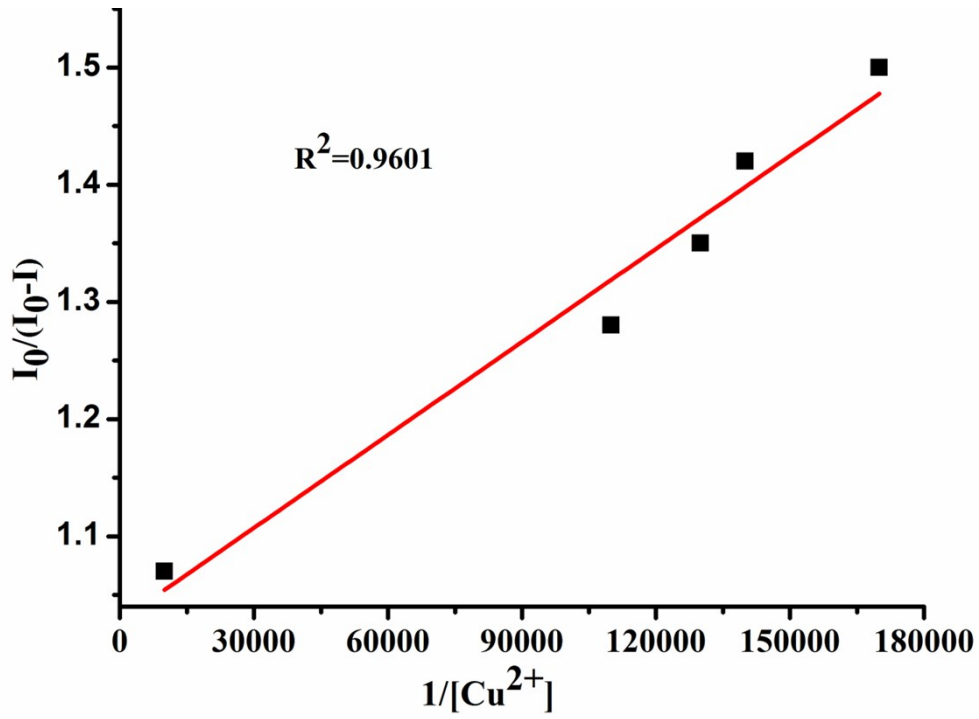

Fig. S14. Stern-Volmer plot for determination of quenching constant of **L1** for Cu^{2+}

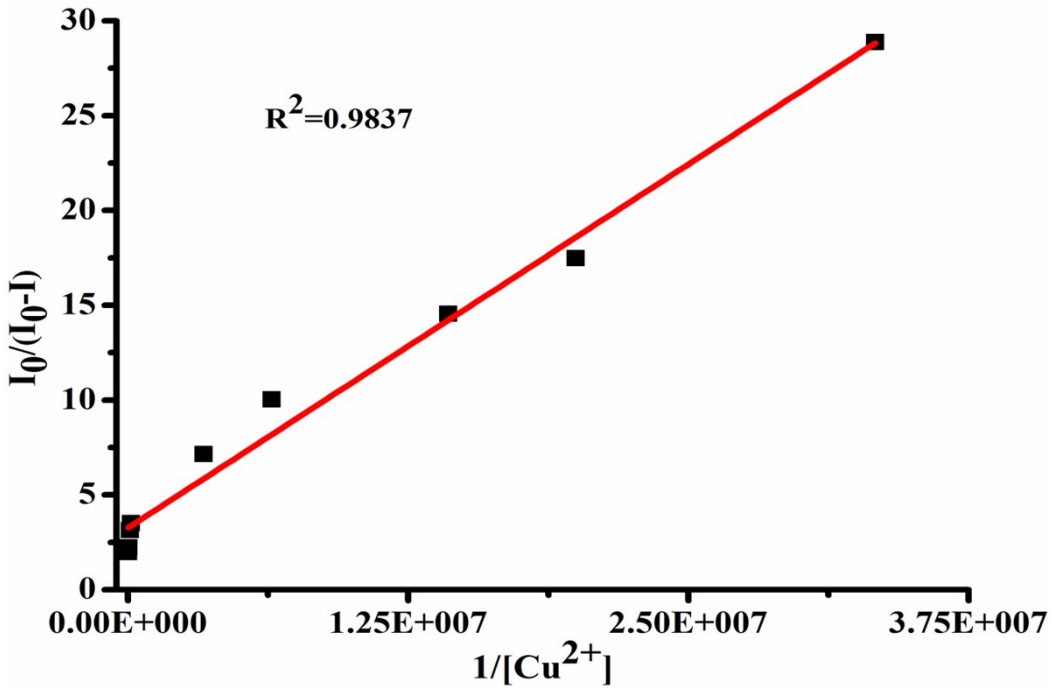

Fig. S15. Stern-Volmer plot for determination of quenching constant of **L2** for Cu^{2+}

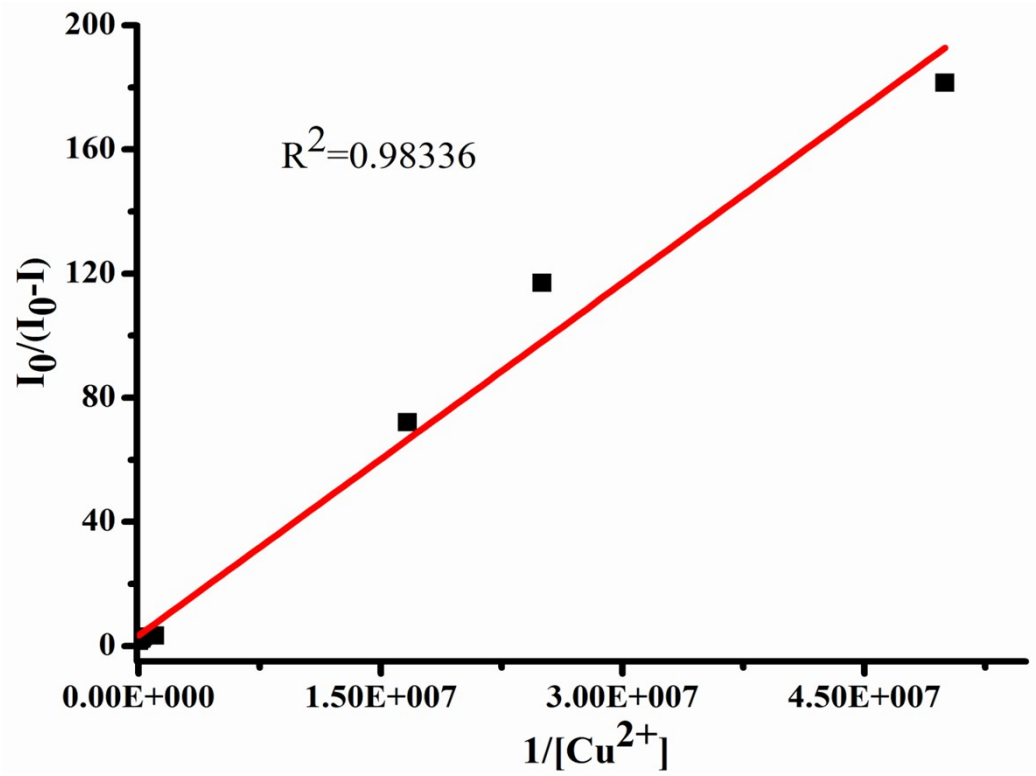

Fig. S16. Stern-Volmer plot for determination of quenching constant of **L3** for Cu^{2+}

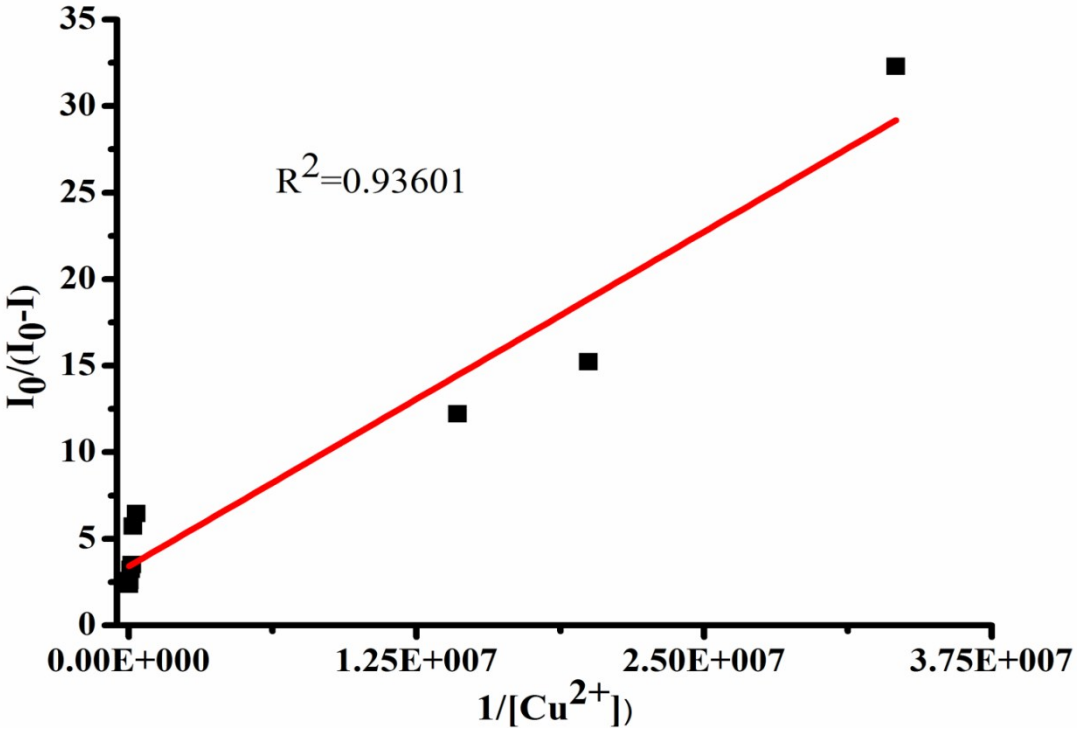

Fig. S17. Stern-Volmer plot for determination of quenching constant of **L4** for Cu^{2+}

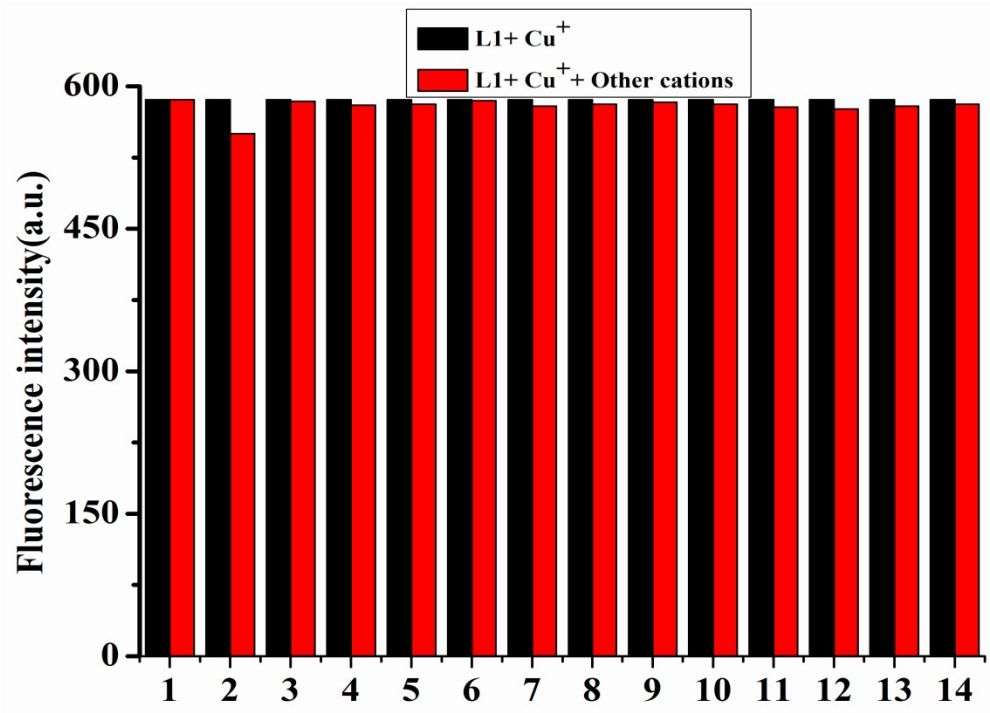

Fig. S18. Cation selectivity of **L1** (1 μM) in $CH_3CN–H_2O$, 1:1 v/v (λ_{ex} = 340 nm). Black bar: emission intensity of the [**L1**+ Cu^+] system; red bar: emission intensity of the [**L1**+ Cu^+] system in presence of 800 μM of different cations, i.e. Blank (1), Cu^{2+} (2), Hg^{2+} (3), Zn^{2+} (4), Pb^{2+} (5), Ag^+ (6), Au^+ (7), Sn^{2+} (8), Cr^{3+} (9), Al^{3+} (10), Fe^{3+} (11), Pd^{2+} (12), Cd^{2+} (13) and Fe^{2+} (14)

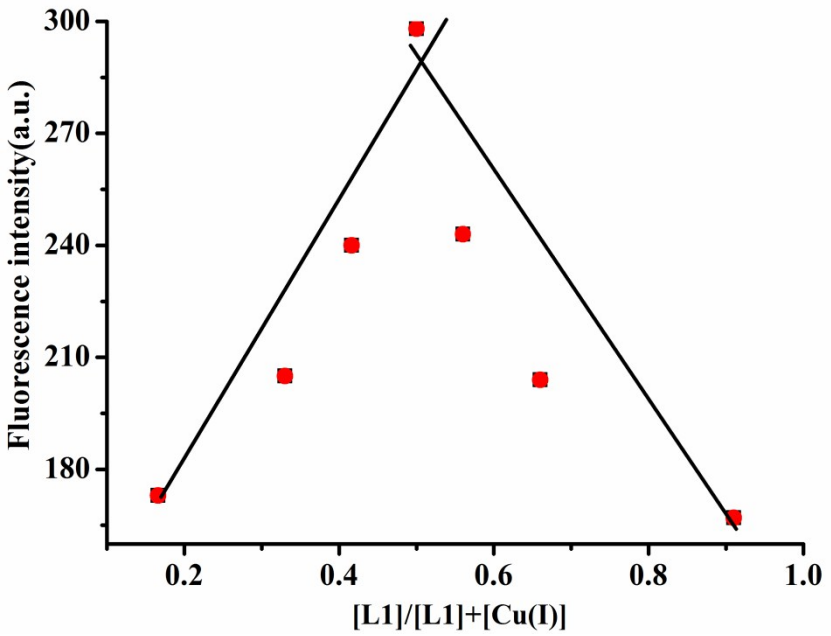

Fig. S19. Job's plot for determination of stoichiometry between **L1** and Cu^+ in CH_3CN/ H_2O (1/1, v/v)

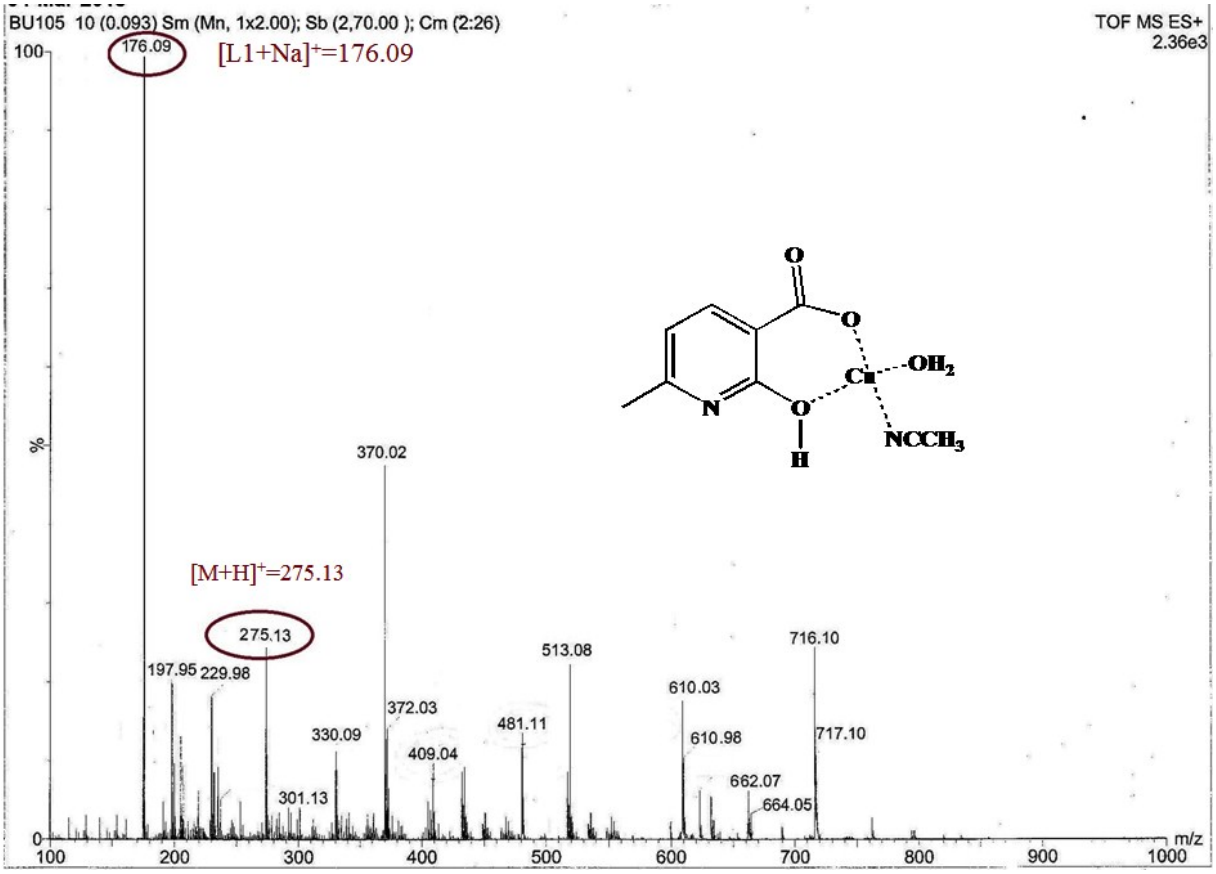

Fig. S20 ESI-MS spectra of the adduct between **L1** and Cu^+ in solution

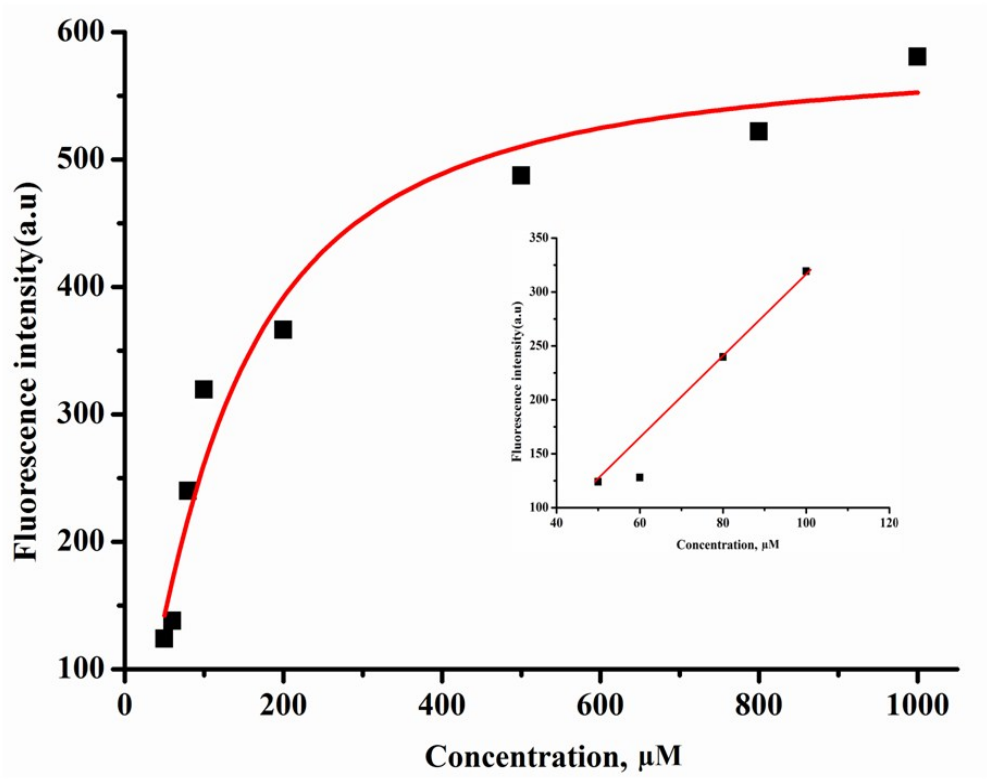

Fig. S21. Emission intensity of **L1** as function of added Cu^+ (50–1000 μM). Inset: linear region, up to 100 μM Cu^+

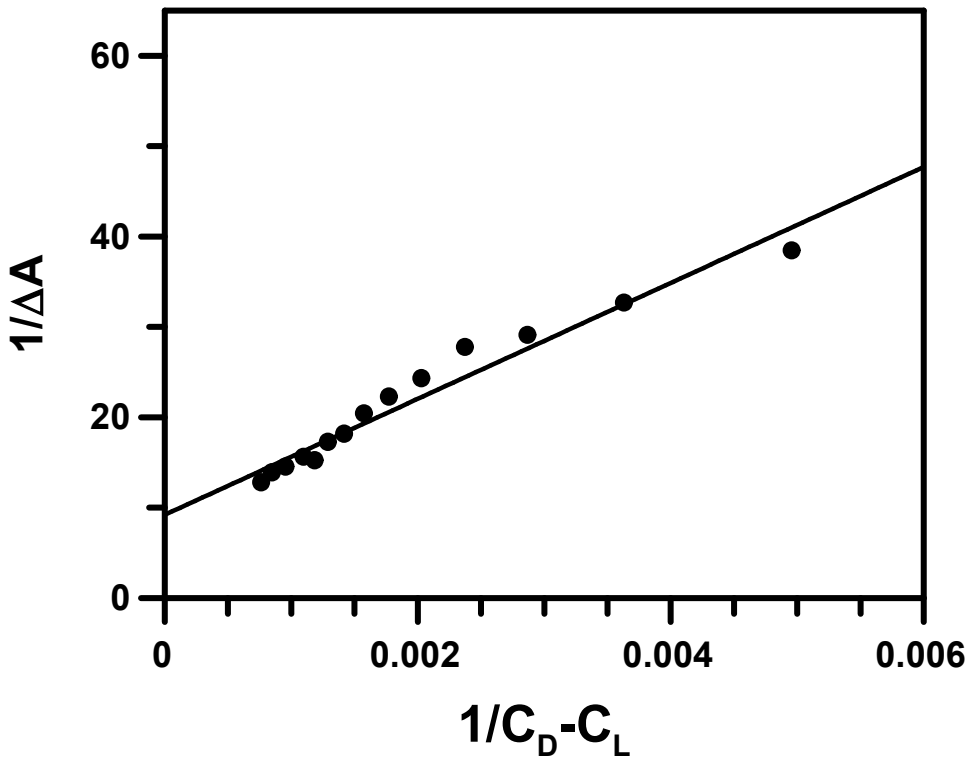

Fig. S22. Double-reciprocal plot for evaluation of apparent binding constant of **C1a** for c t DNA based on UV-Vis titration

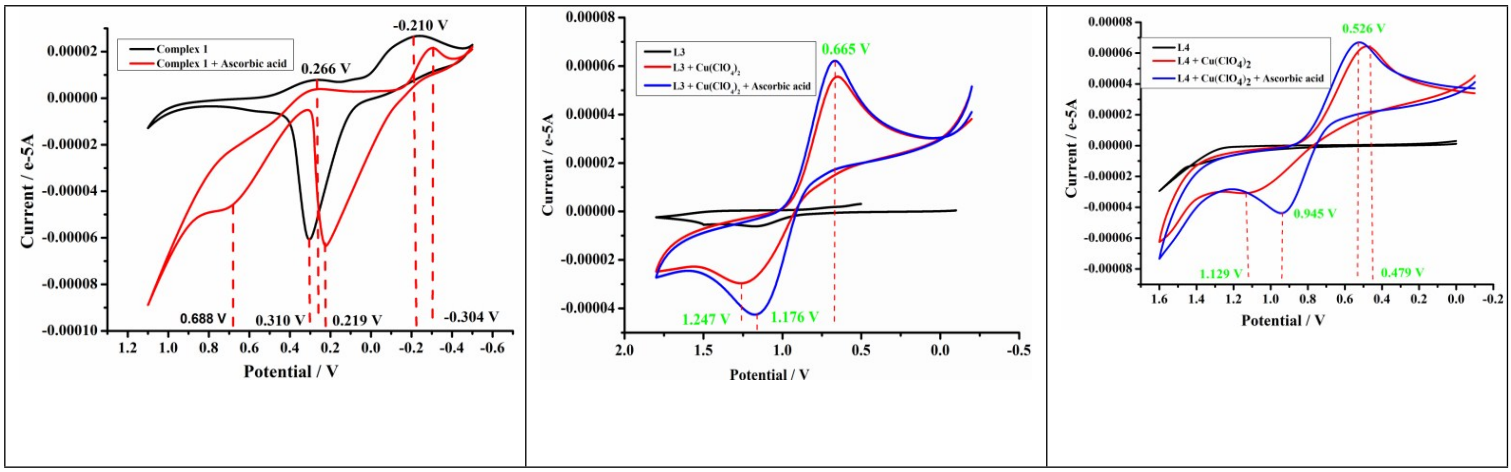

Fig. S23. Cyclic voltammogram of Cu^{2+} complexes in acetonitrile

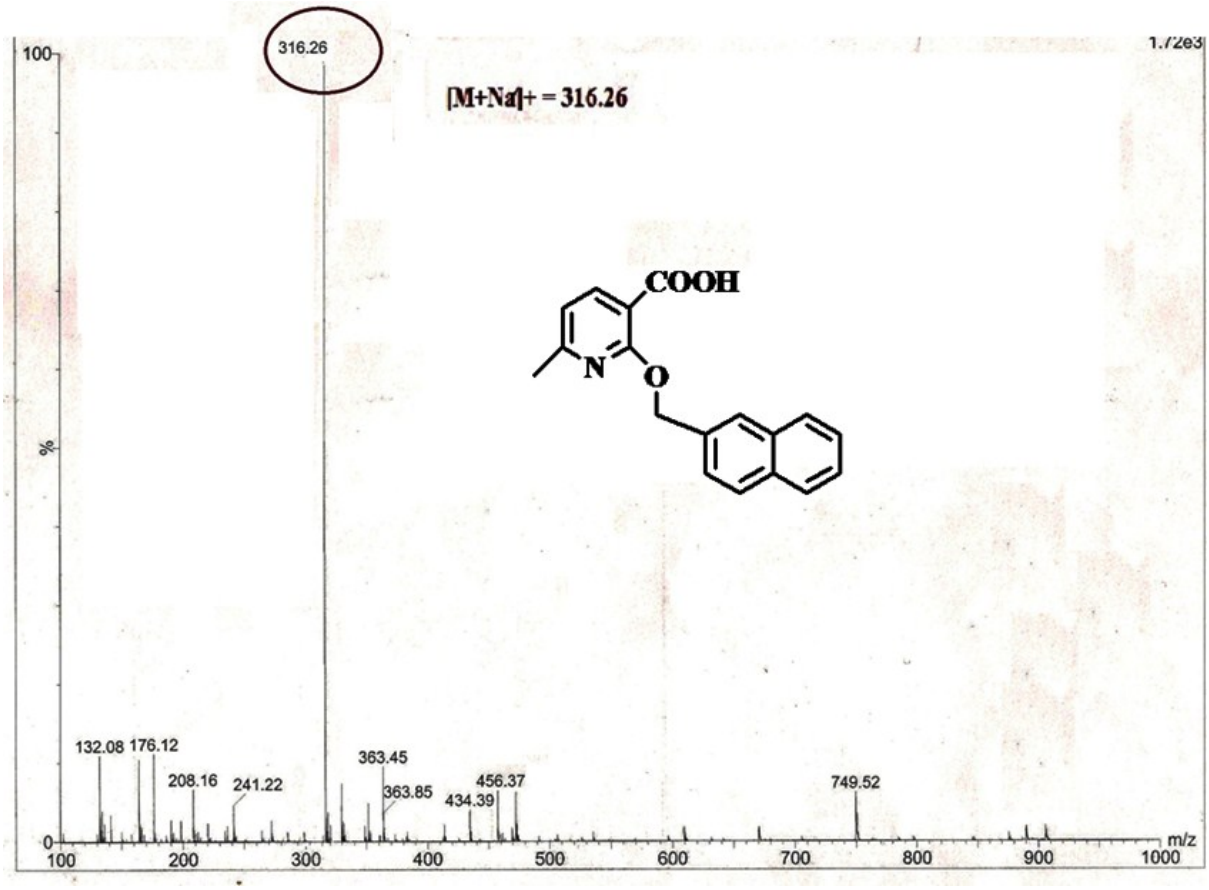

Fig.S24.ESI-MS of **L2**

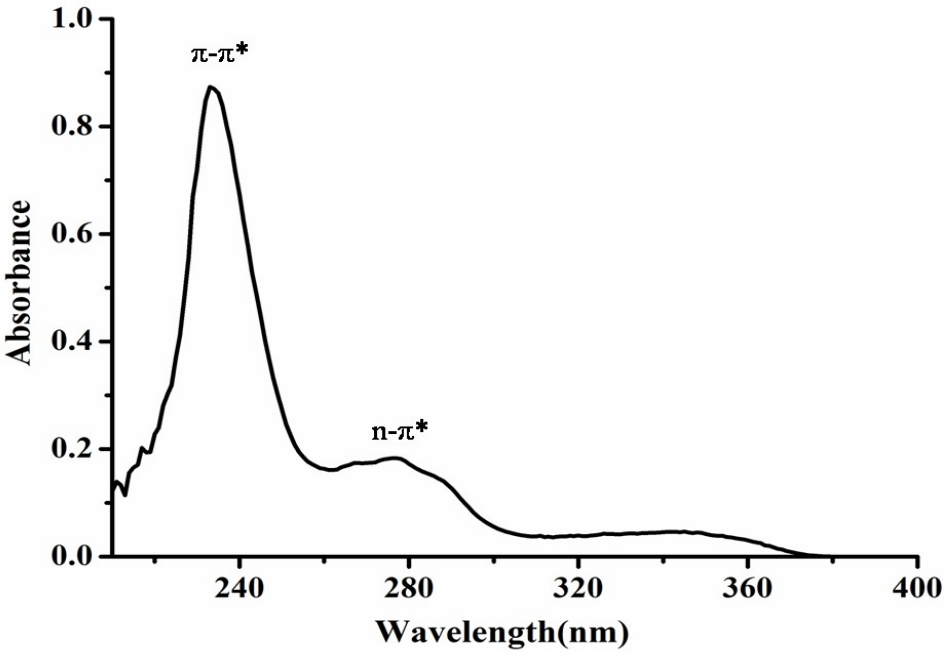

Fig. S25. UV-Vis spectrum of **L2** in acetonitrile

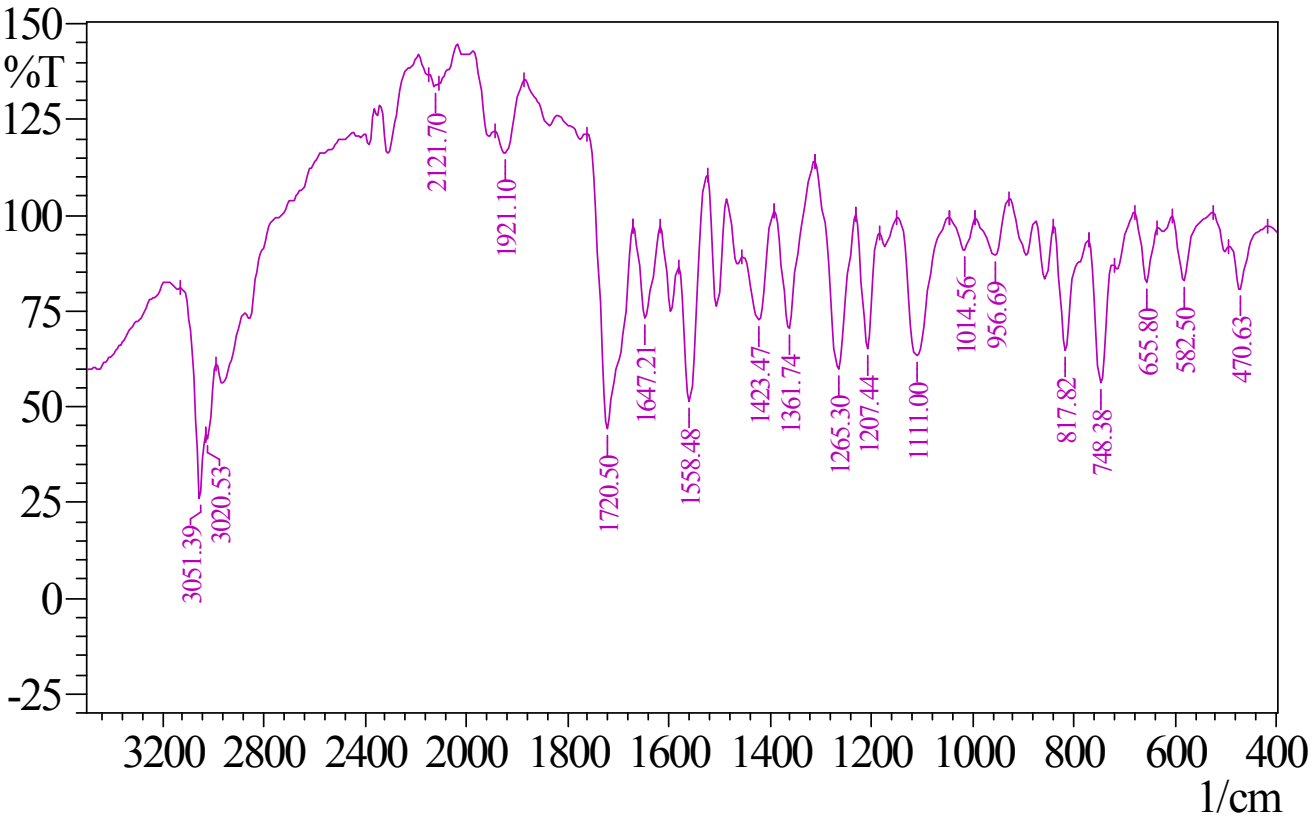

Fig. S26. FTIR spectrum of **L2**

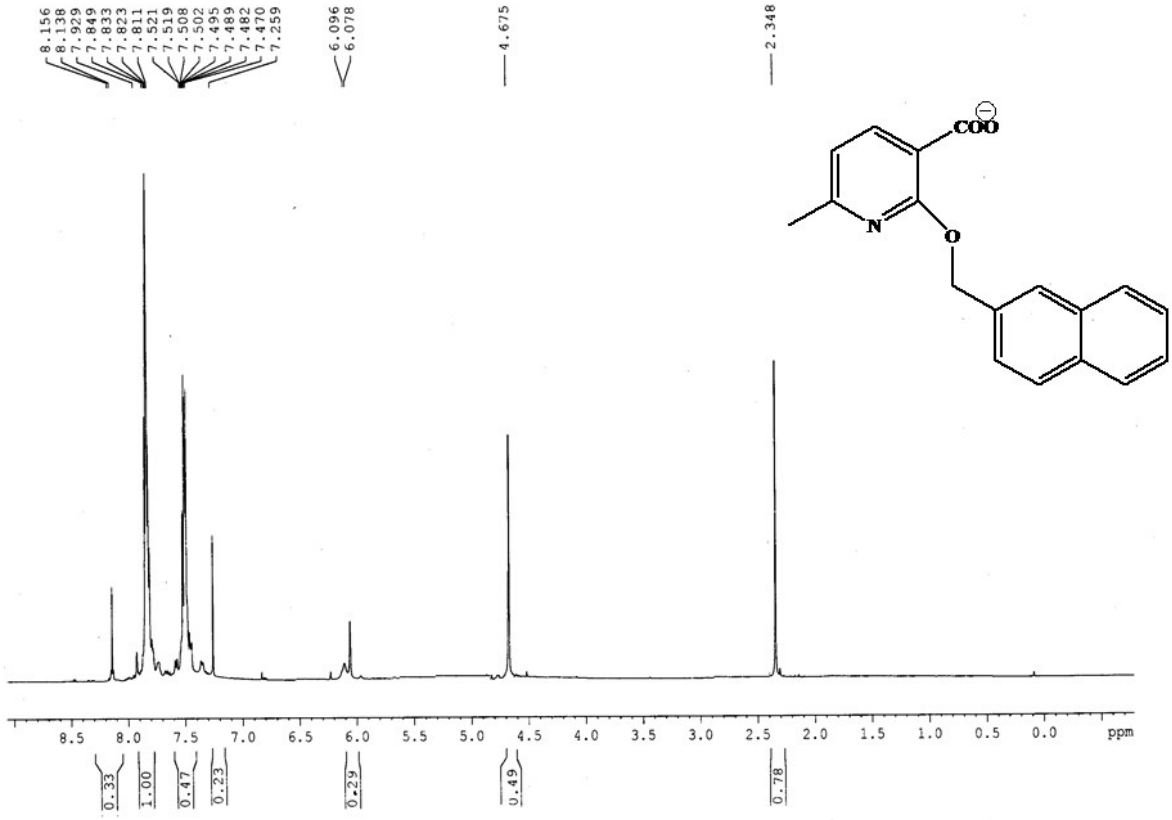

Fig. S27.^{1}HNMR spectrum of **L2** in $CDCl_3$

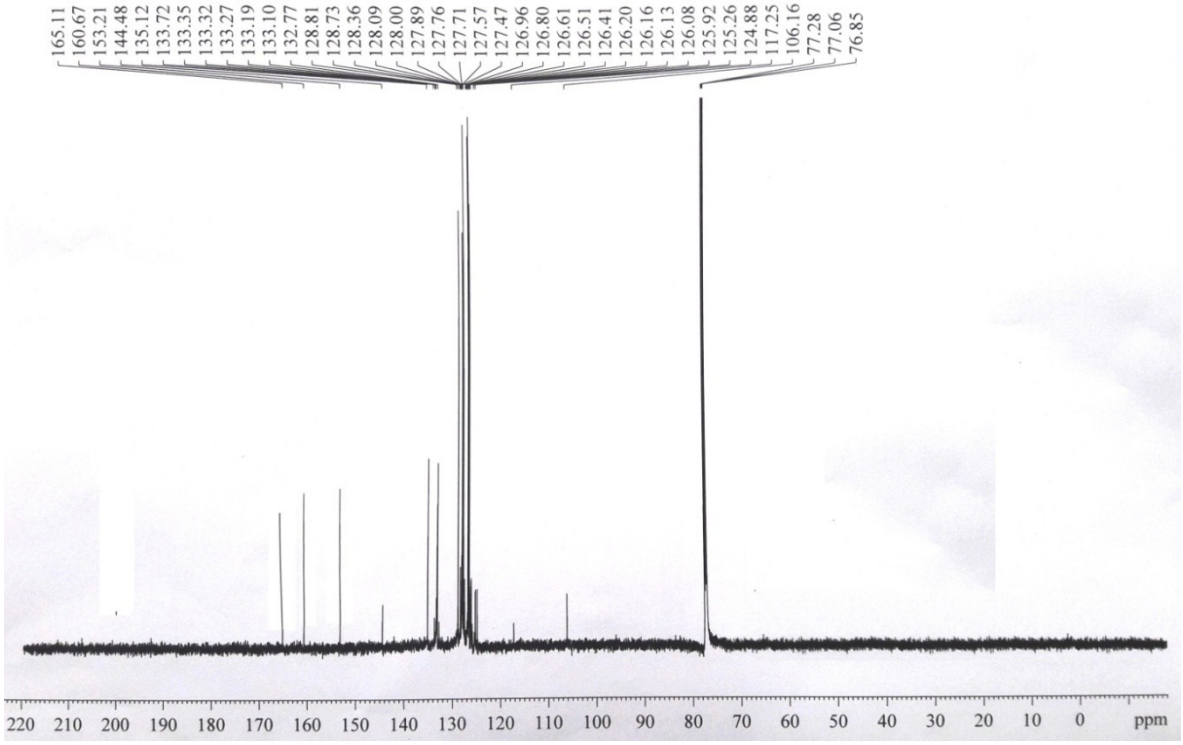

Fig. S28.^{13}CNMR spectrum of **L2** in $CDCl_3$

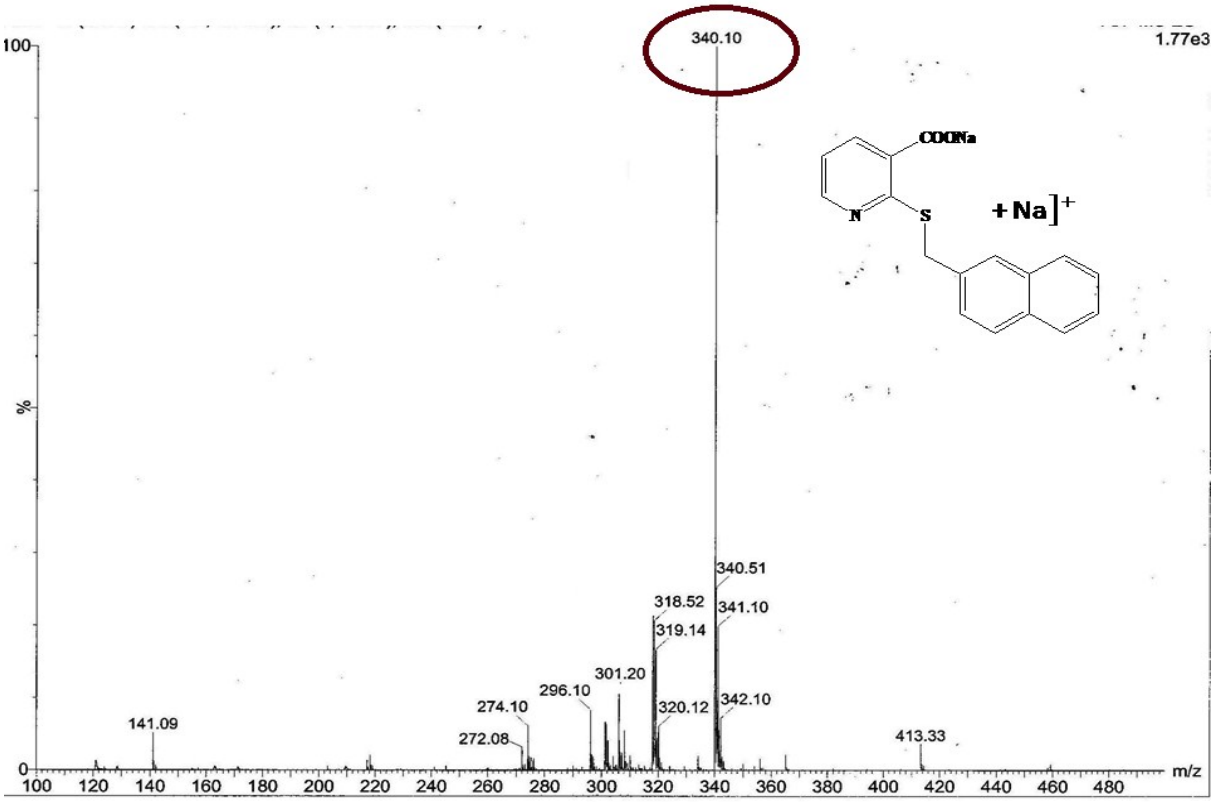

Fig. S29. ESI-MS of **L4**

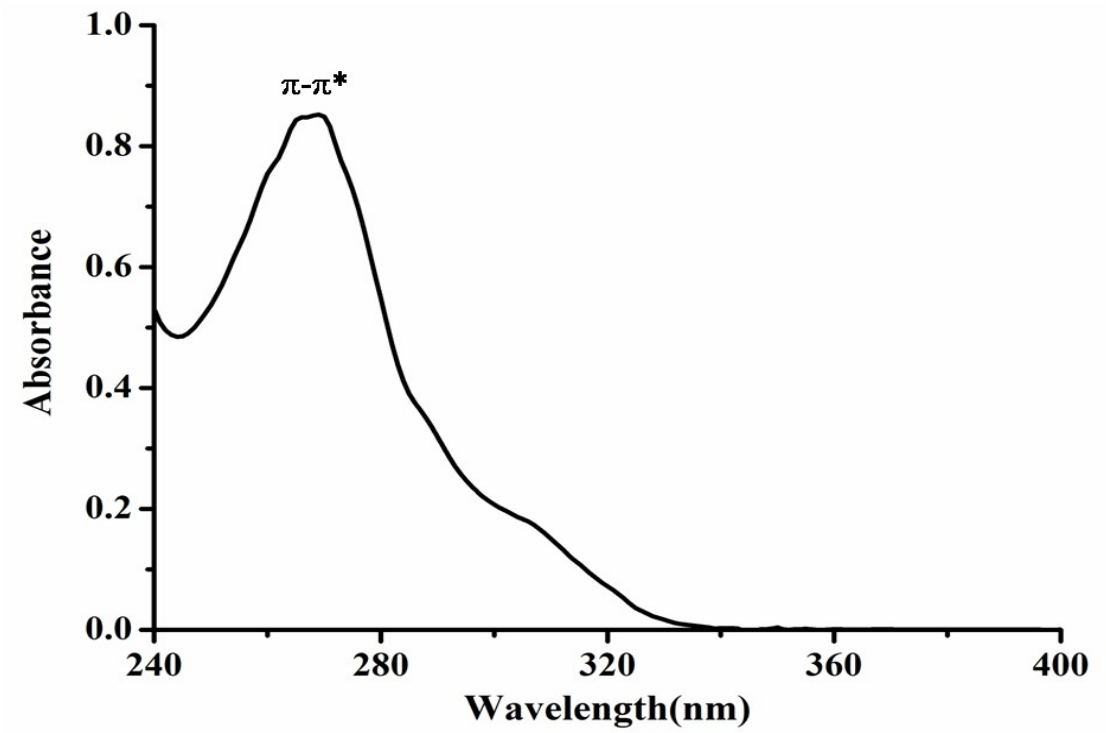

Fig. S30.UV-Vis spectrum of **L4** in acetonitrile

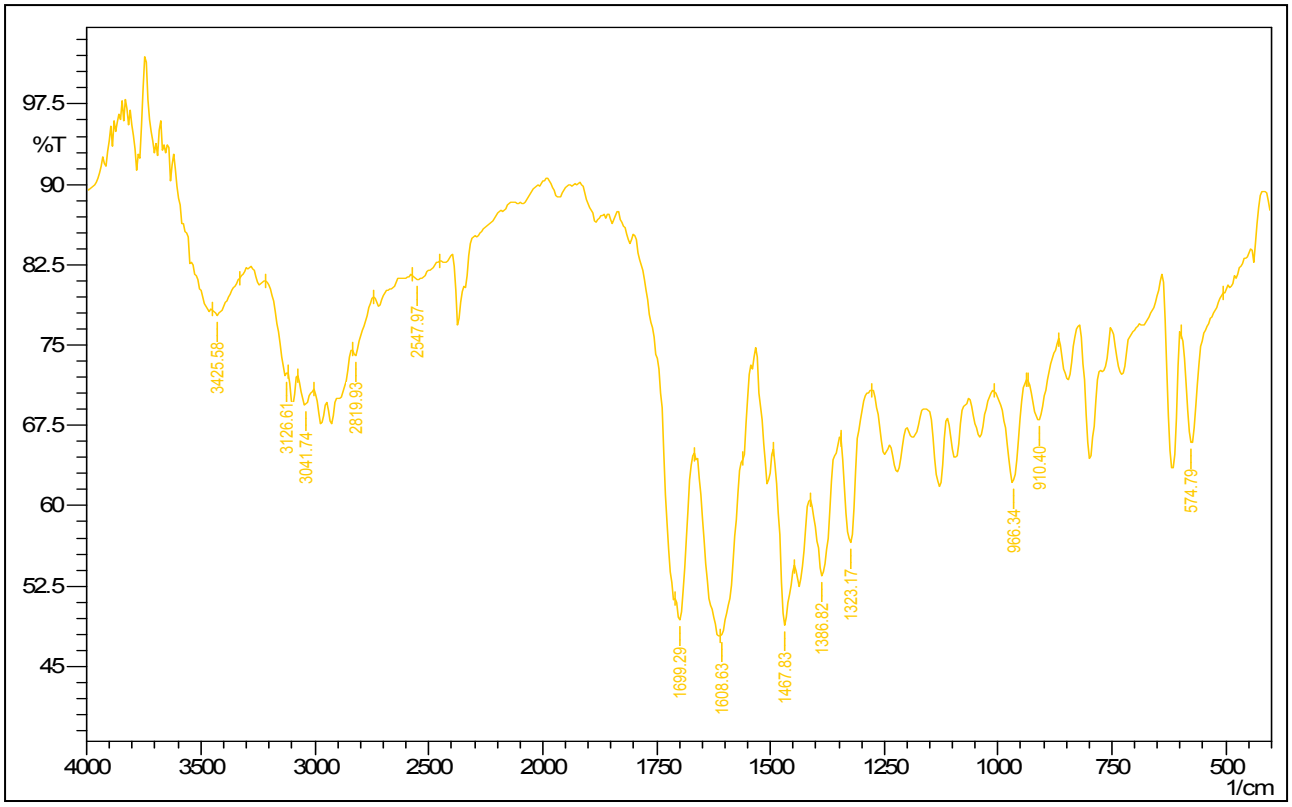

Fig. S31. FTIR spectrum of **L4**

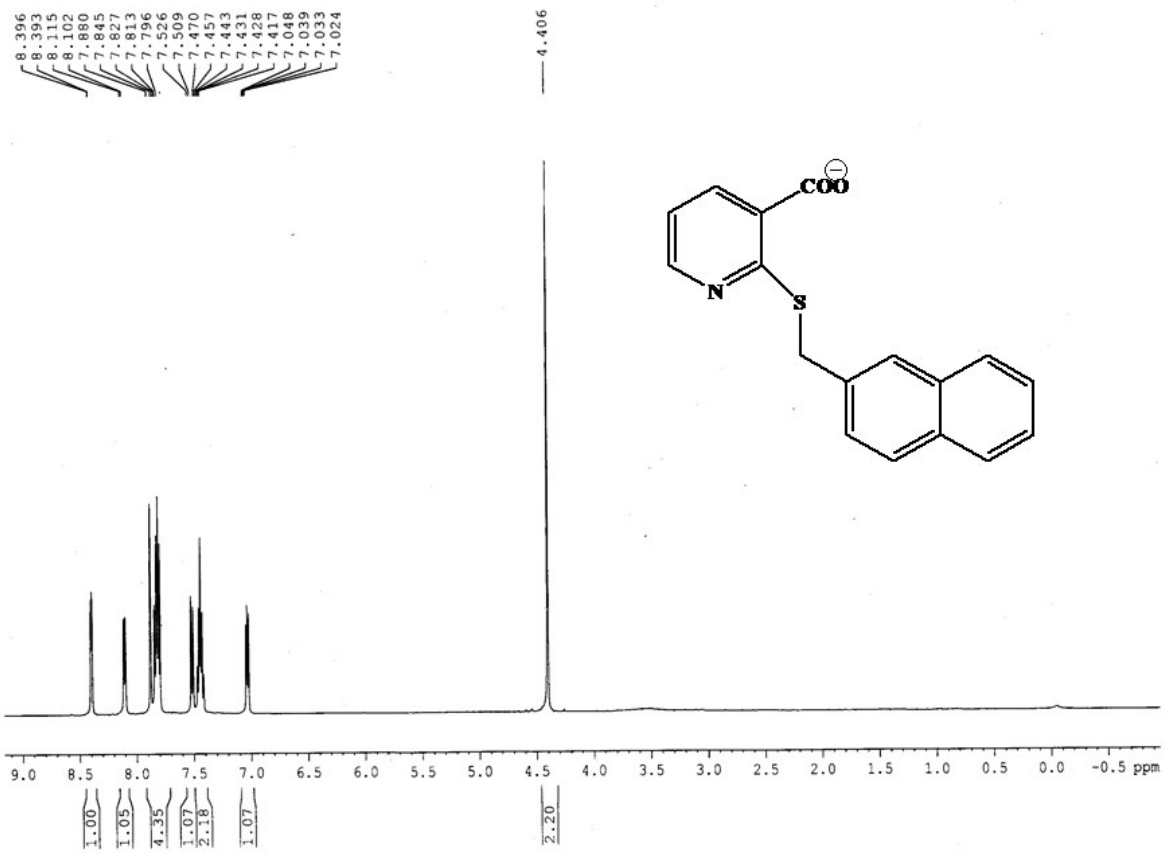

Fig. S32.^{1}HNMR spectrum of **L4** in DMSO-d_6

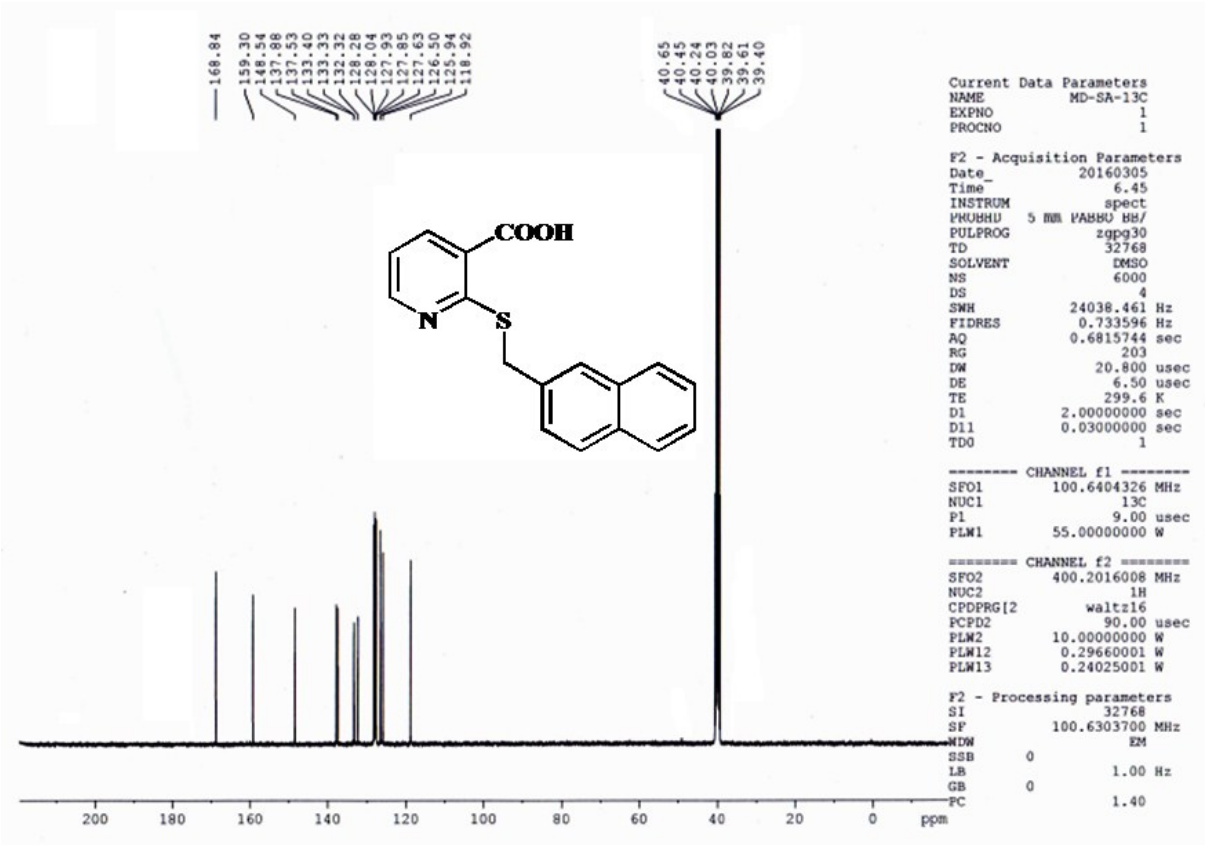

Fig. S33.^{13}CNMR spectrum of **L4** in DMSO-d_6

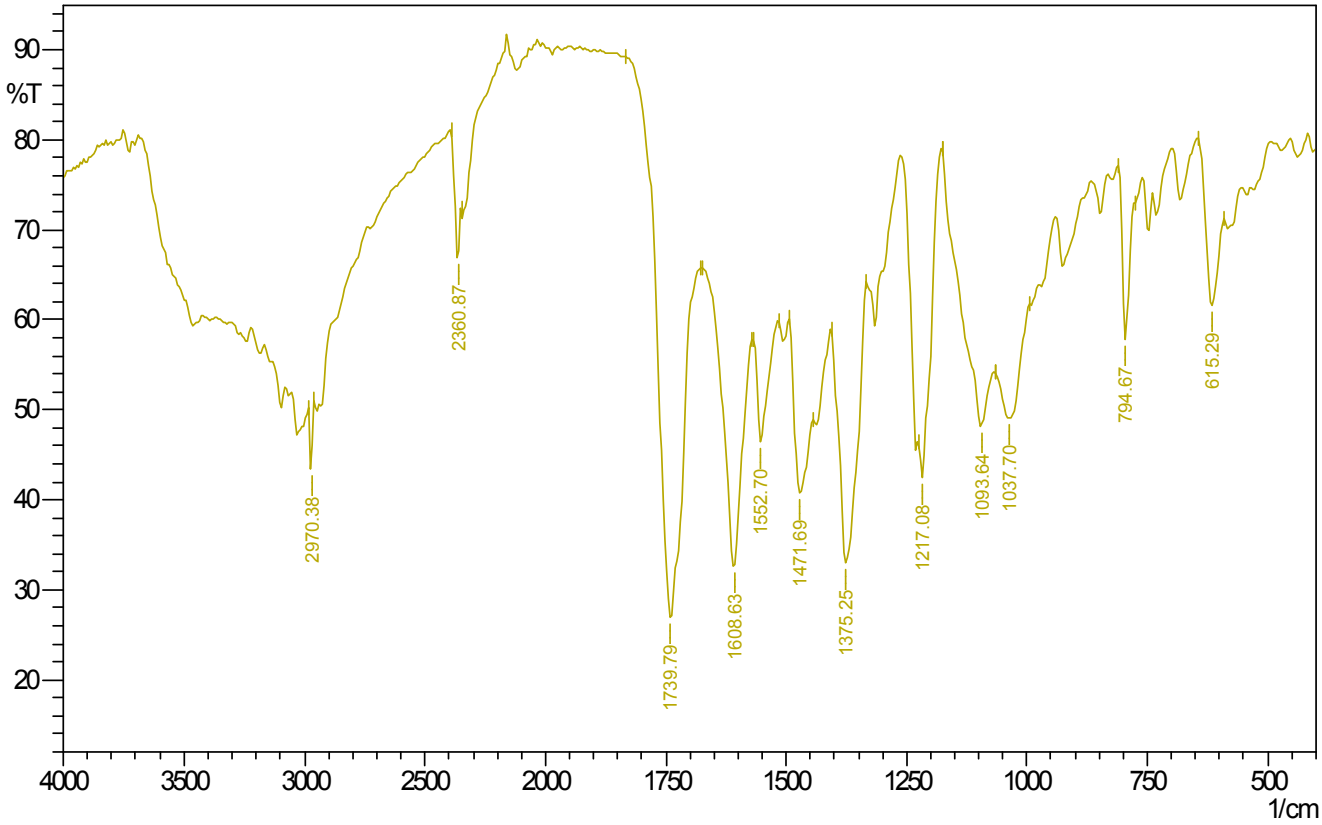

Fig. S34 FTIR spectrum of **C1a**

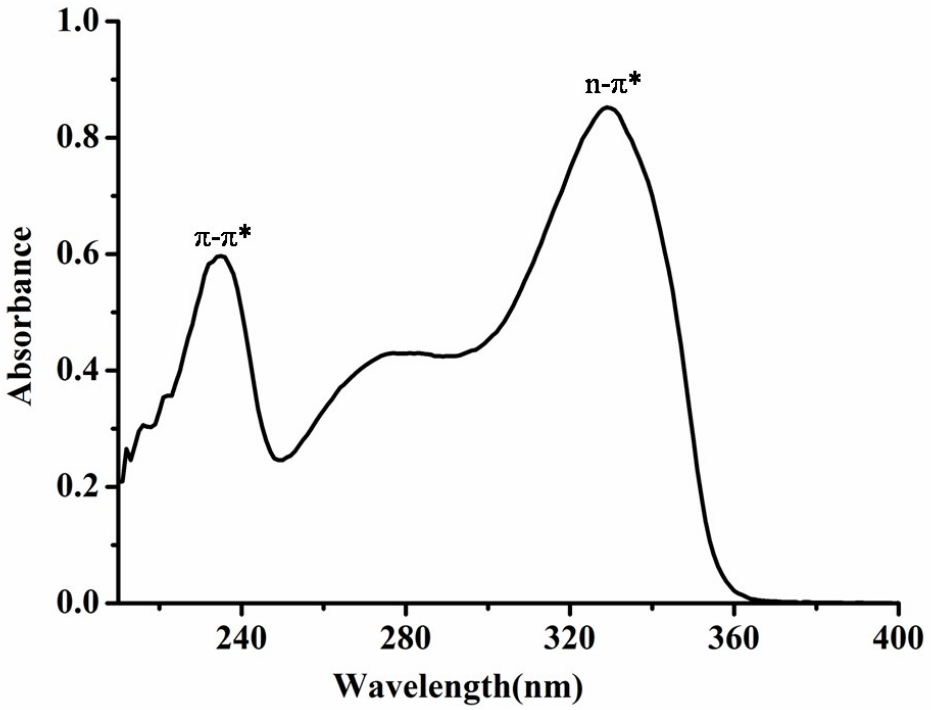

Fig. S35. UV-Vis spectrum of **C1a** in acetonitrile

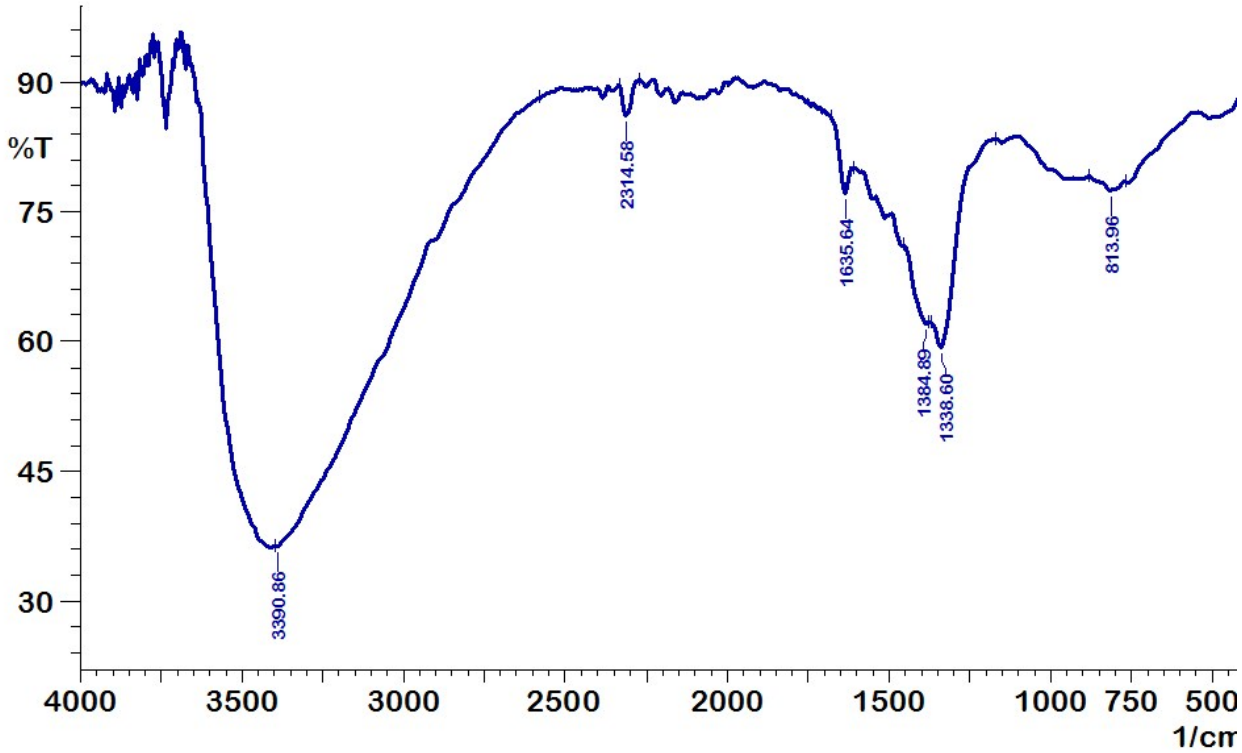

Fig. S36. FTIR spectrum of **C2**

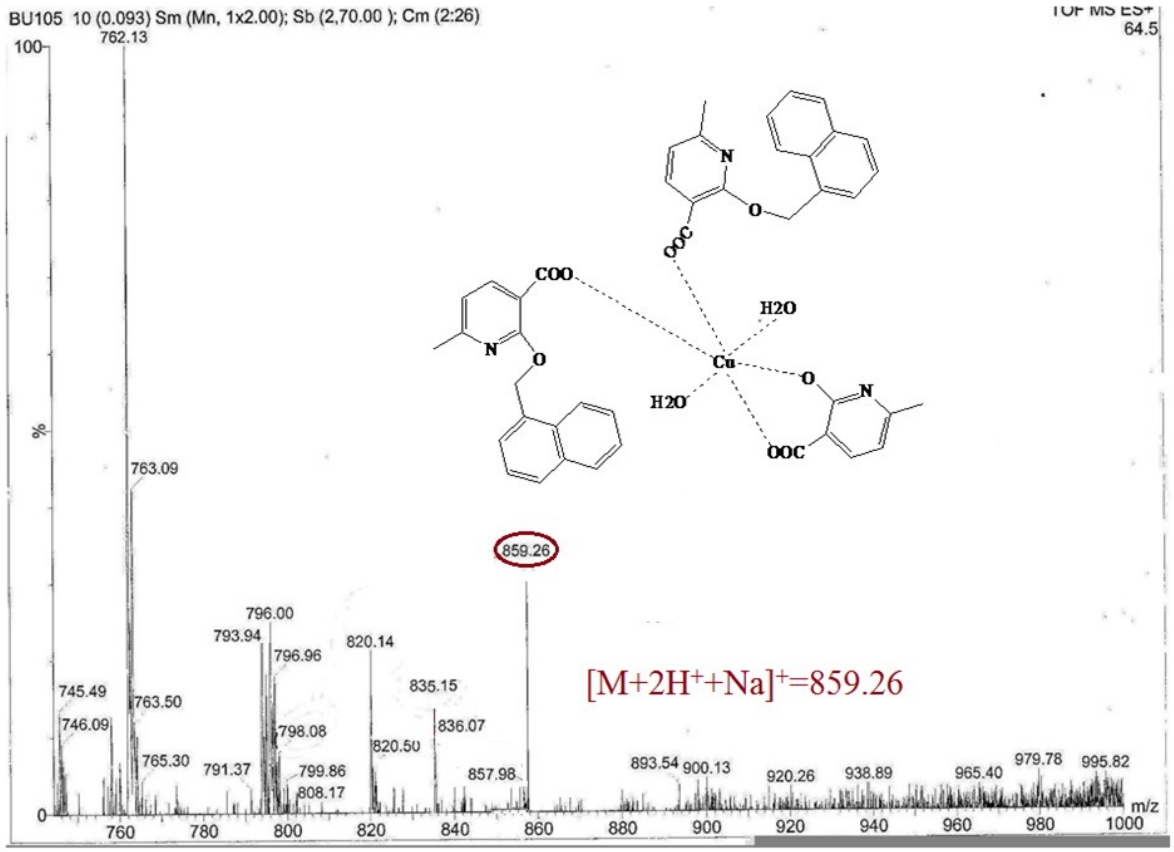

Fig. S37. ESI-MS spectrum of **C2**

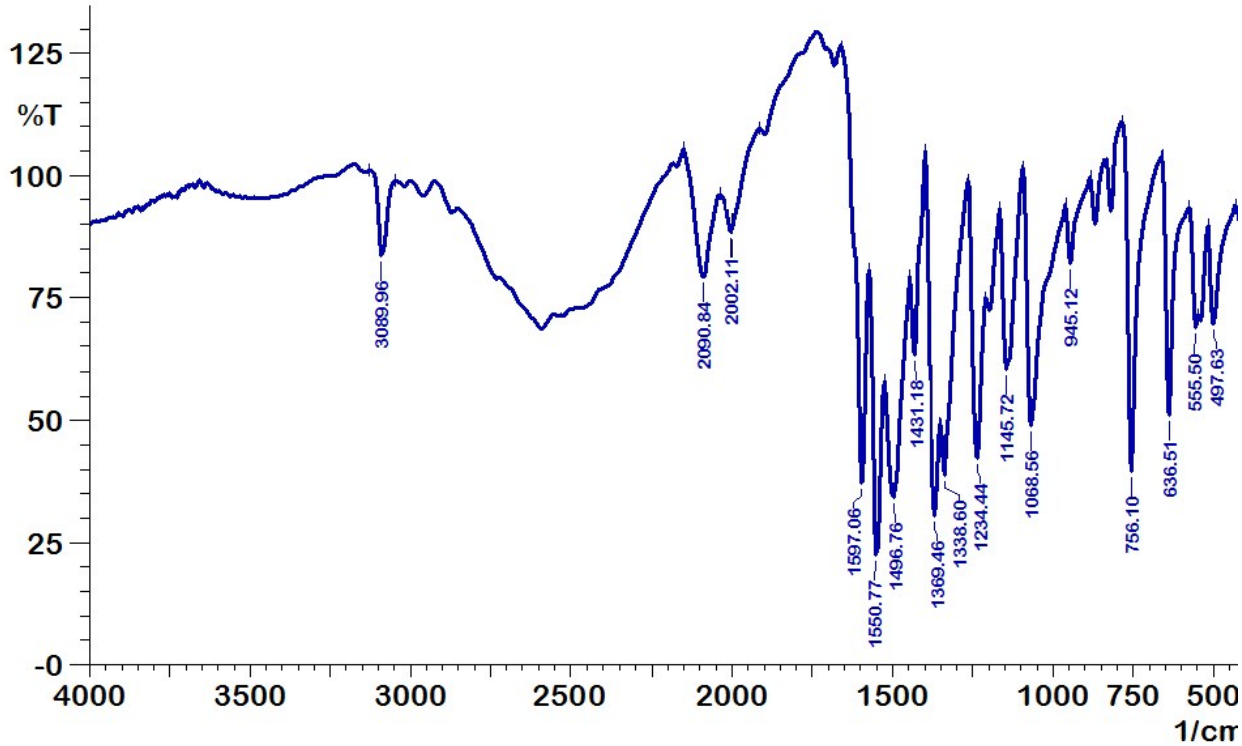

Fig. S38. FTIR spectrum of **C3**

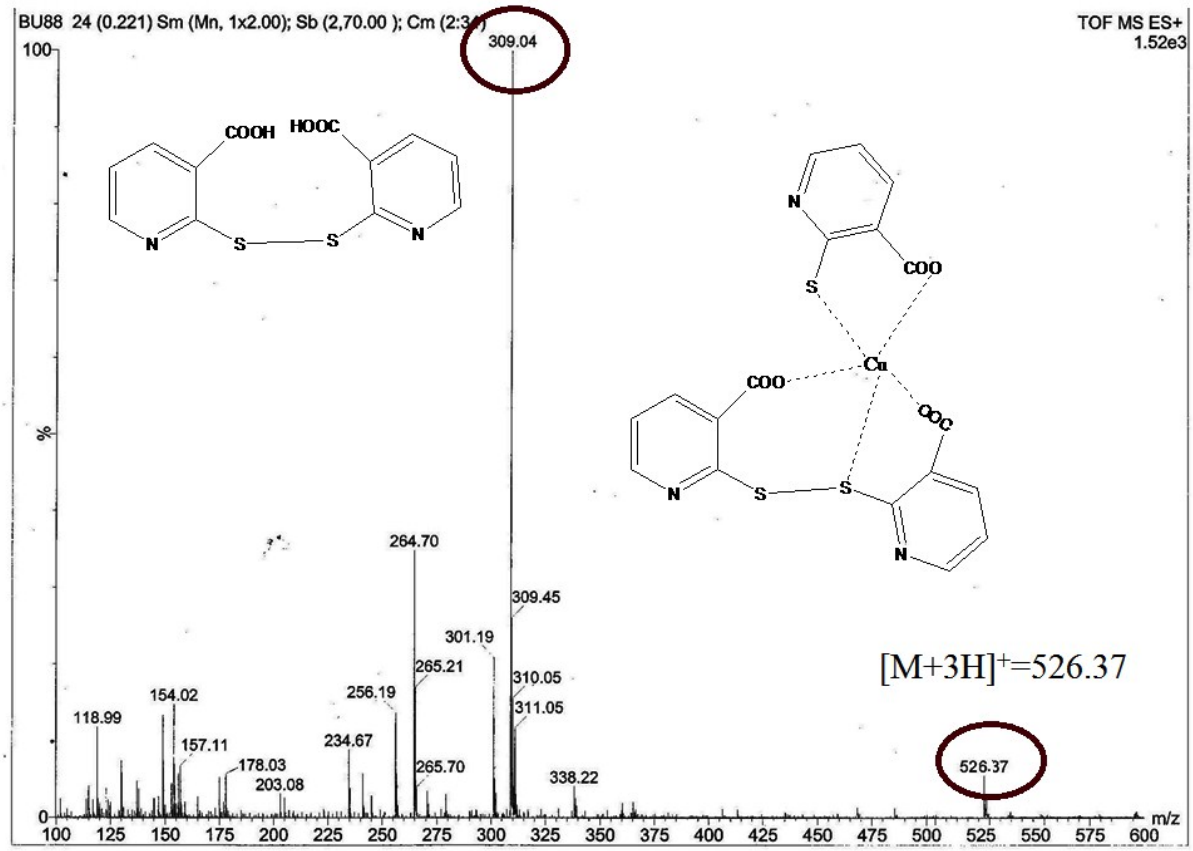

Fig. S39. ESI-MS of **C3**

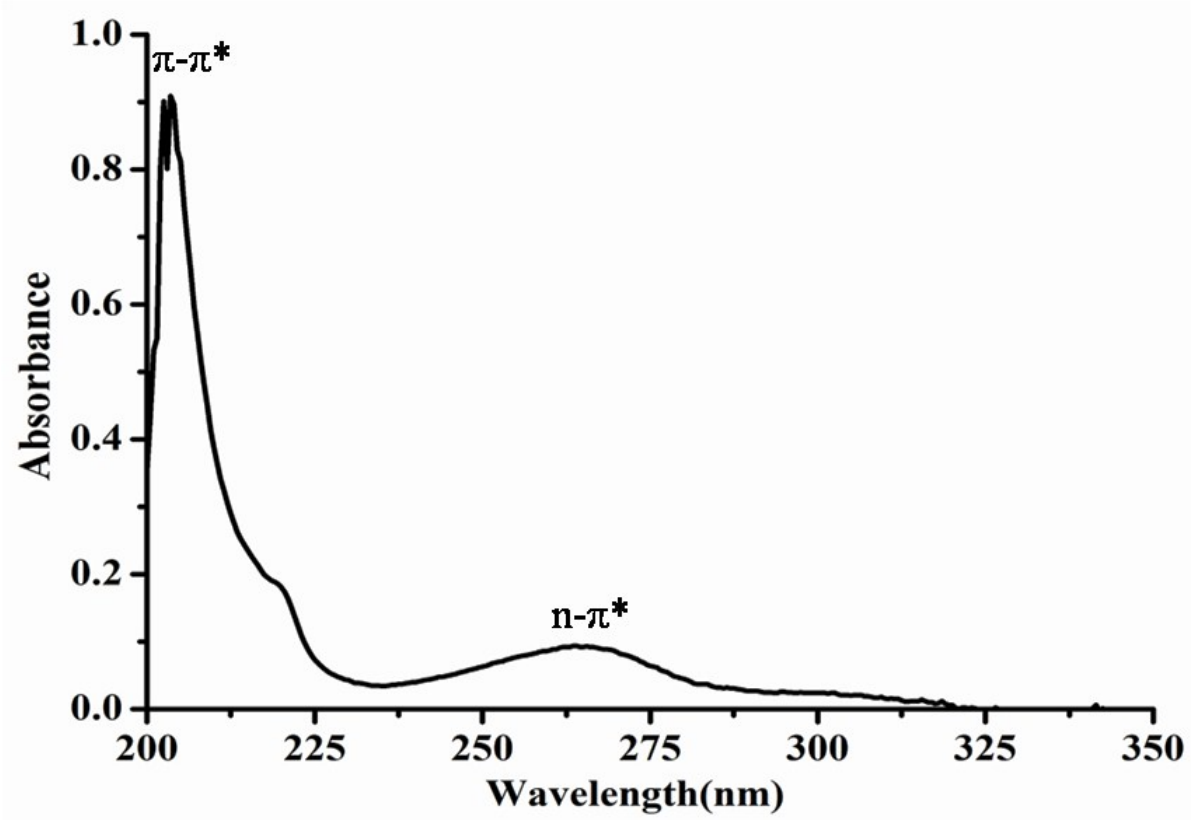

Fig. S40. UV-Vis spectrum of **C3** in acetonitrile

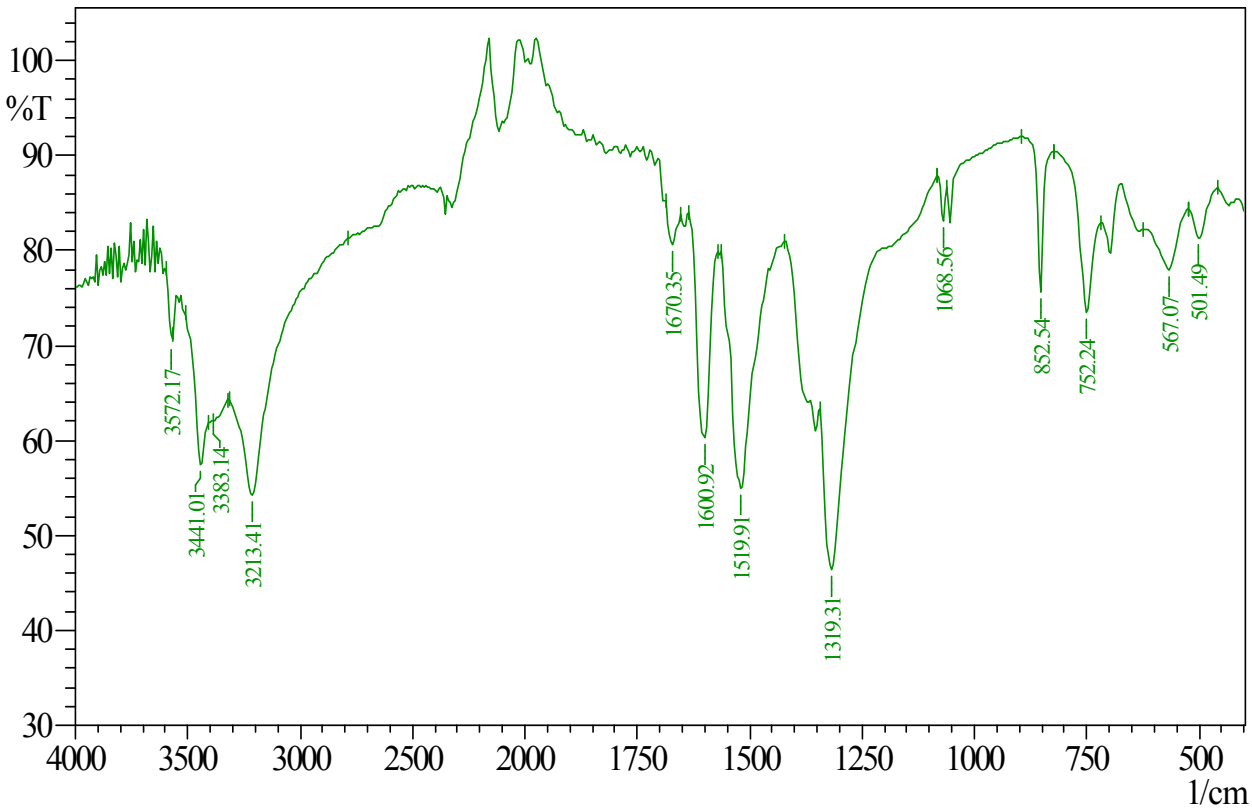

Fig. S41. FTIR spectrum of **C4**

Table S1. Bond lengths and bond angles in the Cu(II) coordination sphere of **C1a**

Molecules	A	B		A	B
		Bond lengths (Å) [a)]			
Cu-O(1)	1.947(2)	1.937(2)	Cu-O(21)	1.925(2)	1.937(2)
Cu-O(10)	1.960(2)	1.937(2)	Cu-O(23)	2.308(3)	2.269(3)
Cu-O(12)	1.951(2)	1.960(5)	Cu-O(*x*)	2.562(3)	2.596(3)
		Bond angles (°)[a)]			
O(1)-Cu-O(10)	90.65(10)	93.24(9)	O(10)-Cu-O(x)	79.82(10)	86.88(10)
O(1)-Cu-O(12)	175.64(11)	175.93(14)	O(12)-Cu-O(21)	92.87(9)	91.57(9)
O(1)-Cu-O(21)	89.19(10)	87.35(10)	O(12)-Cu-O(23)	89.02(9)	92.62(11)
O(1)-Cu-O(23)	87.02(10)	91.43(9)	O(12)-Cu-O(*x*)	81.65(10)	90.97(10)
O(1)-Cu-O(x)	102.16(10)	85.05(10)	O(21)-Cu-O(23)	93.26(10)	99.03(10)
O(10)-Cu-O(12)	87.91(10)	87.42(9)	O(21)-Cu-O(*x*)	91.56(10)	86.98(10)
O(10)-Cu-O(21)	171.15(11)	173.75(12)	O(23)-Cu-O(*x*)	169.70(12)	172.91(12)
O(10)-Cu-O(23)	95.58(10)	87.18(11)			

a) *x* denotes 111 for molecule A and 211 for molecule B.

Table S2. Hydrogen bond dimensions of **C1a**

D-H···A[a)]	H···A (Å)	D···A (Å)	D-H···A (°)
O(3)-H(3A)···O(14A) [1+*x*,*y*,z]	1.60(5)	2.441(3)	170(4)
N(6A)-H(6A)···O(300)	1.96(2)	2.825(4)	173(3)
N(6B)-H(6B) ···O(100)	1.89(2)	2.750(4)	168(4)
O(14B)-H(14B)···O(3B) [-1+*x*,*y*,z]	1.63(7)	2.462(3)	156(8)
N(17A)-H(17A)···O(200) [1-*x*,-1/2+*y*,1-z]	1.976(17)	2.852(4)	174(2)
N(17B)-H(17B)···O(400)	1.898(17)	2.777(4)	173(4)
O(23A)-H(23A)···O(10B) [1-*x*,-1/2+*y*,1-z]	2.01(3)	2.804(3)	163(3)
O(23A)-H(23A)···O(12B) [1-*x*,-1/2+*y*,1-z]	2.50(3)	3.032(3)	124(3)
O(23A)-H(23B)···O(3B) [2-*x*,-1/2+*y*,1-*z*]	1.97(4)	2.791(4)	178(4)
O(23B)-H(23C)···O(300) [1-*x*,1/2+*y*,1-*z*]	2.03(3)	2.825(4)	158(4)
O(23B)-H(23D)···O(12A) [1-*x*,1/2+*y*,1-*z*]	2.29(3)	3.103(3)	166(4)
O(100)-H(101)···O(131)	1.98(4)	2.774(4)	159(5)
O(100)-H(102)···O(23A) [1-*x*,1/2+*y*,1-*z*]	2.04(5)	2.753(4)	144(4)
O(200)-H(201)···O(121)	2.06(2)	2.885(5)	172(5)
O(200)-H(202)···O(231) [1-*x*,1/2+*y*,1-*z*]	2.15(3)	2.928(4)	158(5)
O(300)-H(301)···O(211) [-1+*x*,*y*,-1+*z*]	2.18(4)	2.974(5)	161(4)
O(300)-H(302)···O(21B) [-1+*x*,*y*,-1+*z*]	2.09(4)	2.855(4)	152(4)
O(400)-H(401)···O(10A) [*1*+*x*,*y*,1+z]	2.23(3)	2.987(4)	151(4)
O(400)-H(401)···O(111) [*1*+*x*,*y*,1+z]	2.48(5)	3.024(4)	124(3)
O(400)-H(402)···O(221) [2-*x*,1/2+*y*,2-*z*]	2.16(3)	2.928(4)	155(3)

a) D and A mean hydrogen bond donors and acceptors, respectively.

Table S3. Selected bond lengths (Å) and bond angles (º) of **C1b**

Bond lengths			
Cu(1)-C(l1)	2.673(3)	Cu(1)-O(11)	2.780(13)
Cu(1)-O(1)	1.968(3)	Cu(1)-O(1W)	1.973(5)
Cu(2)-O(2)	1.898(3)	Cu(2)-O(3)	1.933(3)
Cu(2)-O(2W)	2.237(6)		
Bond angles			
O(1)-Cu(1)-O(1)*	180.0	C(l1)-Cu(1)-O(1)	95.95(10)
O(1)*-Cu(1)-O(1W)	98.8(2)	O(1)-Cu(1)-O(1W)	81.2(2)
O(1W)-Cu(1)-O(1W)*	180.0(4)	O(1)*-Cu(1)-Cl(1)	84.05(10)
O(1)-Cu(1)-Cl(1)	95.95(10)	C(l1)-Cu(1)-C(l1)	180.0
O(1)-Cu(1)-O(11)	82.69(17)	O(11)-Cu(1)-O(11)*	180.0
O(1)*-Cu(1)-O(11)	97.31(17)	O(11)-Cu(1)-O(1W)	80.1(4)
O(2)-Cu(2)-O(2)**	172.2(2)	O(2)-Cu(2)-O(3)**	86.92(14)
O(2)-Cu(2)-O(3)	91.96(14)	O(3)-Cu(2)-O(3)**	163.52(19)
O(2)-Cu(2)-O(2W)	103.46(16)	O(2)-Cu(2)-O(2W)**	84.37(15)
O(3)-Cu(2)-O(2W)	94.0(2)	O(3)-Cu(2)-O(2W)**	102.2(2)

* and ** stand for 3/2-*x*,-y,1/2-z and x,-1/4-y,3/4-z, respectively.

Table S4. Selected bond lengths (Å) and angles (º) of**C4**

Bond lengths			
Cu(1)-O(8)	2.602(8)	Cu(1)-O(39)^{i}	1.947(2)
Cu(1)-O(9)^{i}	1.964(2)	Cu(1)-O(1w)	2.197(2)
Cu(1)-O(38)	1.951(2)	Cu(1)-Cu(1)^{i}	2.603(8)
Bond angles			
O(8)-Cu(1)-O(1W)	91.61(10)	O(9)^{i}-Cu(1)-Cu(1)^{i}	85.23(7)
O(8)-Cu(1)-O(9)^{i}	169.31(8)	O(9)^{i}-Cu(1)-O(39)	90.46(9)
O(8)-Cu(1)-O(38)	88.72(9)	O(38)-Cu(1)-O(1W)	86.61(10)
O(8)-Cu(1)-O(39)^{i}	89.04(9)	O(38)-Cu(1)-Cu(1)^{i}	80.94(6)
O(8)-Cu(1)-Cu(1)^{i}	84.07(6)	O(38)-Cu(1)-O(39)^{i}	169.23(9)
O(9)^{i}-Cu(1)-O(38)	89.79(9)	O(39)^{i}-Cu(1)-O(1w)	104.10(10)
O(9)^{i}-Cu(1)-O(1W)	98.88(10)	O(39)^{i}-Cu(1)-Cu(1)^{i}	88.34(6)
O(1W)-Cu(1)-Cu(1)^{i}	166.80(7)		

a) ^{i} stands for the symmetry operation *-x, -y, -z*

Table S5 Crystal data and refinement parameters

Compound	**L1**	**C1a**	**C1b**	**C4**
Molecular formula	L1	$[Cu(L1)(H_2O)(SO_4)]$. $2H_2O$	$[Cu_2(L^1)_2(H_2O)_3]_n(NO_3)_nCl_n \cdot nH_2O$	$[Cu_2(L4)_4(H_2O)_2]$.1.12(H_2O)
Empirical formula	$C_7H_7NO_3$	$C_{14}H_{20}CuN_2O_{13}S$	$C_{14}H_{20}ClCu_2N_3O_{13}$	$C_{68}H_{54.24}Cu_2N_4O_{11.12}S_4$
Formula weight	153.14	519.92	600.86	1360.66
Temperature(K)	293(2)	100(2)	100	110(2)
Crystal system	Orthorhombic	Monoclinic	Orthorhombic	Monoclinic
Space group	*P*bca	$P2_1$	F_{ddd}	$P2_1/c$
Unitcell dimensions				
a (Å)	7.39817(15)	8.7731(5)	13.0670(9)	19.4562(31)
b (Å)	13.0179(2)	13.7449(7)	17.8555(12)	15.7960(25)
c (Å)	14.3767(3)	16.6071(9)	36.247(3)	10.1007(16)
β (º)	90.00	93.648(2)	90	103.170(2)
V ($Å^3$)	1384.60(5)	1998.52(2)	8457.0(10)	3022.6(9)
Z	8	4	16	2
D_{calc} (g/cm^{-3})	1.469	1.728	1.888	1.495
□□(mm^{-1})	0.117	1.270	2.212	0.909
F(000)	640	1068	4864.0	1402.1
Crystal size (mm^3)	0.30×0.25×0.20	0.18×0.12×0.03	0.20 x 0.22 x 0.23	0.37×0.36×0.19
θ range for data collection (º)	3.47-25.35	2.33-27.18	0.454	2.43-23.16
Index ranges	$-8 \le h \le 8$, $-15 \le k \le 15$, $-17 \le l \le 17$	$-11 \le h \le 11$, $-17 \le k \le 17$, $-21 \le l \le 21$	$-16 \le h \le 13$, $-22 \le k \le 21$, $-45 \le l \le 45$	$-24 \le h \le 23$, $0 \le k \le 19$, $0 \le l \le 12$
Reflections collected	16333	40334	14568	24837
Independent reflections, [R_{int}]	1242, [0.0296]	8790, [0.0294]	2169, [0.054]	5953, [0.0566]
Final *R* indices				
R_1, wR_2 [I>2σI]	0.0378, 0.1093, [1169]	0.0255, 0.0654, [8279]	0.0433, 0.1202, [1569]	0.0433, 0.0991, [4434]
R_1, wR_2 (all data)	0.0394, 0.1108	0.0283, 0.0664	0.0433(1569), 0.1202(2169)	0.0694, 0.1123
Largest diff. peak and hole ($eÅ^{-3}$)	0.200 and -0.157	0.60 and -0.58	0.76, and -0.58,	0.441 and -0.545

References

1. R. Kubin, *J. Lumin*., 1983, **27**, 455.
2. S. Roy, R. Banerjee and M. Sarkar, *J. Inorg. Biochem*., 2006, **100**, 1320.
3. M. Tachibana and M. Iwaizumi, *J. Inorg. Biochem*., 1987, **30**, 141.
4. S. Mukherjee, P. Das and S. Das, *J. Phy.Org. Chem*., 2012, **25**, 385.

5. P. Das, C. K. Jain, S. K. Dey, R. Saha, A. DuttaChowdhury, S. Roychowdhury, S. Kumar, H. K. Majumdar and S. Das, *RSC Advances*., 2014, **4**, 59344.
6. P. Das, P. S. Guin, P. C. Mandal, M. Paul, S. Paul and S. Das, *J. Phy.Org. Chem*., 2011, **24**, 774.
7. P. S. Guin, S. Das and P. C. Mandal, *J. Inorg. Biochem*., 2009, **103**, 1702.
8. S. Das, A. Saha and P. C. Mandal, *Talanta* 1996, **43**, 95.
9. H. Beraldo, A. G. Suillerot and L. Tosi, *Inorg. Chem*., 1983, **22**, 4117.
10. M. Tachibana, M. Iwaizumi and S. Tero-Kobuta, *J. Inorg. Biochem*., 1987, **30**, 133.
11. F. Morazzoni and A. Gervasini, *Inorg. Chim. Acta*., 1987, **136**, 111.
12. S. Mukherjee, P. Das and S. Das, *J. Phy.Org. Chem*., 2012, **25**, 385.
13. S. Roy, R. Banerjee and M. Sarkar, *J. Inorg. Biochem*., 2006, **100**, 1320.
14. S. Chakraborti, B. Bhattacharyya and D. Dasgupta, *J. Phys. Chem*., B 2002, **106**, 6947.
15. G. Scatchard, N. Y. Ann. *Acad. Sci*., 1949, **51**, 660.
16. O. V. Dolomanov, L. J.Bourhis, R. J. Gildea, J. A. K. Howard and H. Puschmann, *J. Appl. Crystallogr*., 2009, **42**, 339.